Food and Agriculture Organization
of the United Nations

The global distribution of human-induced land degradation and areas at risk

SOLAW21 Technical background report

The global distribution of human-induced land degradation and areas at risk

SOLAW21 Technical background report

by
Ruben Coppus
Independent consultant

Food and Agriculture Organization of the United Nations
Rome, 2023

Required citation:

Coppus, R. 2023. *The global distribution of human-induced land degradation and areas at risk. SOLAW21 Technical background report.* Rome, FAO. https://doi.org/10.4060/cc2843en

ISBN 978-92-5-137166-4

Cover photograph: ©FAO/Salvator Ndabirorere

Contents

Tables

Figures

Acknowledgements

The report has greatly benefited from comments and suggestions of earlier versions received from Riccardo Biancalani and Monica Petri at FAO, and Luca Montanarella and Panos Panagos at the Joint Research Centre. Access to the GAEZ data was facilitated by Federica Chiozza.

Special thanks go to Freddy Nachtergaele for the substantive discussions and his support in obtaining valuable geospatial data.

Jakob Burke is acknowledged for his constructive criticism of later versions and many thanks go to Ruth Raymond for copy-editing the final report. SOLAW 21 was managed by Rosalud De La Rosa and coordinated by Feras Ziadat.

Key messages

- Nearly all inhabited parts of the world are subject to some form of human-induced land degradation.
- There is a clear overlap of areas with water-related issues and human-induced land degradation.
- The correlation between commonly used indicators, such as decreasing land productivity or increased soil erosion, and the occurrence of land degradation is relatively weak.
- Cropland is strongly affected by human-induced land degradation, in particular irrigated land.
- Grazing is the most common occurring driver of human-induced degradation, followed by accessibility and agricultural expansion.
- Land degradation is evenly distributed over drylands and humid areas.
- In half of the protected areas worldwide, the biophysical status is deteriorating.

1. Introduction: updating the Global Land Degradation Information System

Land degradation is a global environmental and socioeconomic problem recognized by various United Nations conventions and the Sustainable Development Goals (SDGs). SDG target 15.3 (combat desertification, restore degraded land and soil) explicitly mentions the concept of land degradation neutrality (LDN) and is linked to the implementation of the United Nations Convention to Combat Desertification (UNCCD). Unsustainable agricultural management is a major cause of land degradation and there is growing concern that it will lead to decreasing productivity, compromising SDG 2.3: improvement of livelihoods and food security (Gerten *et al.,* 2020).

To achieve these targets and goals, reliable information is needed on the global distribution of land degradation and the extent to which agricultural land and forests are at risk. Although land degradation is generally recognizable in the field, it cannot be measured directly or monitored with earth observation techniques. Land degradation is the result of complex local biophysical conditions and socioeconomic drivers, which are difficult to capture on a single map. A complicating factor is that land degradation is perceived differently by local populations and concerned stakeholders, based on their interests (FAO, 2013). Such perceptions are influenced by trade-offs between biophysical and environmental gains versus social or economic losses or vice versa (Fisher *et al.*, 2018).

The global land degradation assessment of the Intergovernmental Science-Policy Platform on Biodiversity and Ecosystem Services (IPBES) describes land degradation as the many processes that drive the decline of biodiversity, ecosystem functions or ecosystem services (Fisher *et al.,* 2018). The Intergovernmental Panel on Climate Change (IPCC) defines it as a negative trend in land condition caused by direct or indirect human-induced processes, including climate change, expressed as long-term reduction or loss of at least one of the following: biological productivity, ecological integrity or value to humans (Olsson *et al.,* 2019). According to both definitions, land degradation is restricted to human-induced processes.

The Land Degradation Assessment in Drylands programme (LADA) (FAO, 2013) defined land degradation as a process that reduces the capacity of land to provide ecosystem goods and services for beneficiaries and stakeholders. In LADA's Global Land Degradation Information System (GLADIS) (Nachtergaele *et al.,* 2011) the status of the provisioning capacity of the ecosystems is seen to be as important as its reduction. Consequently, both a negative change in status and a low provisioning capacity were associated with degradation, regardless of the underlying conditions and processes. Following the GLADIS approach (Nachtergaele *et al.,* 2011), this report identified the current capacity of the land to provide ecosystem services and goods, referred to as status, and the ways in which that has changed in the past 10 to 30 years, referred to as trends. The combined status and trends map shows the areas that are at risk.

GLADIS was criticised for not distinguishing between a decline in status caused by natural drivers and a decline driven by human interference. Drivers are external factors that trigger environmental change. They can affect nature directly, such as soil compaction due to trampling by cattle, or indirectly, such as land use change due to fluctuating world market prices. The origin of direct drivers – also known as pressures – can be natural (e.g.,

earthquakes, volcanic eruptions, hurricanes, pests) or anthropogenic (e.g., agricultural expansion, deforestation, fire, invasive species, mining, infrastructure, industrial development) origin (Barger *et al.,* 2018). This study takes a first step towards separating natural processes from man-made change by including the pressure of direct human drives on agricultural land and ecosystems.

Status, trends and the pressure of direct drivers are three dimensions that, especially in combination, provide a better understanding of the distribution, causes and processes of land degradation. For example, low biophysical status does not necessarily mean that an ecosystem is degraded, as it may be due to unfavourable climatic, soil and terrain conditions. Status combined with trends, however, will reveal whether the ecosystem is in decline (a negative trend) or improving (a positive trend). Areas with low status due to a negative trend are considered at risk. A negative general trend suggests degradation, but without knowledge of the specific human-induced pressure, the nature of the decline is unknown. Trends combined with drivers will reveal how much pressure from human activity is exerted on the system (Cherlet *et al.,* 2018) and whether the decline is of anthropogenic origin or not. A decline caused by human interference is classified as human-induced land degradation.

For this report, two options were chosen to study the decline in the biophysical status of land: areas at risk and human-induced land degradation. The former stresses the impact of decline and the latter focuses on the nature of the decline. The approach was applied to assess the distribution of degradation processes across global land cover and to identify agricultural land and forests at risk.

2. Methodology: a multidimensional approach

2.1 Approach

Land degradation is a process of decline driven by human-induced processes. The decline can be assessed by quantifying or qualifying a change in status over time. Overall status and trend indices were determined using an adapted GLADIS methodology (Nachtergaele *et al.,* 2011). GLADIS uses a geographic information system (GIS) approach that calculates status and trend indices separately for biomass, soil health, water quantity, biodiversity, economic services and cultural services. Combining the six components provides overall status and trend indices.

For the purposes of this study, 'status' reflects current biophysical conditions and focuses on soil, water and vegetation/land cover properties (see Table 1). Trends refers to changes over time and not to processes. For example, the mean soil erosion rate is included in the status analysis and changes in soil erosion rate are used as an input layer for the overall trend. Due to a limited number of input layers, the overall status and trend indices were calculated directly, without determining separate indices for the various components. In addition, the 'convergence of evidence' concept, developed by Cherlet *et al.* (2018) for the World Atlas of Desertification (WAD) was adapted and applied for direct anthropogenic drivers of degradation. The approach uses abductive reasoning and argues that a combination of pressures prompted by human activities can lead to environmental change. For example, when rangeland is burned to produce fresh forage for livestock, three direct anthropogenic drivers of land degradation may coincide: fire, grazing and the invasion of exotic species. The sum of these pressures is known as the cumulative pressure by anthropogenic drivers.

Maps recently published in peer-reviewed journals were used as input layers. The criteria for selecting input layers were availability, readiness to be used, relevance according to the literature (e.g., Nachtergaele *et al.,* 2011; FAO and ITPS 2018; Cherlet *et al.,* 2018; IPBES, 2018; IPCC, 2019) and date of publication. Most available layers only needed minor adjustments to be used as input layer and were current, except for groundwater (Richts *et al.,* 2008), native and invasive species (Ellis *et al.,* 2012), wind erosion (Ginoux *et al.,* 2012) and fire (Archibald *et al.,* 2013), for which no up-to-date information was found. Above-ground biomass, agricultural expansion, deforestation, fire, forest biomass change, grazing density, population density change and water stress change were compiled for this study. Water stress change was calculated with the water stress index by Qin *et al.* (2019), which is based on scarcity, flexibility and variability. Certain key drivers are missing or underrepresented (e.g., land use change, climate change, agricultural management, industrial development and pollution); this will be discussed in more detail in Sections 2.7, 3.4.3 and 4.2.

Table 1. Selected input layers for biophysical status, trend and cumulative pressure by drivers

	Soil	Water	Vegetation	Demography
Status	Nutrient availability Soil carbon content Water erosion Wind erosion	Groundwater recharge SFV water stress	Native species richness Above ground biomass	Built-up cover
Trend	Soil erosion change Soil protection change	Fresh water change SFV water stress change	Change in land productivity Forest biomass change	Population density change
Driver	Accessibility, Agricultural expansion, Deforestation, Fire, Grazing density, Invasive species			

This study integrates the three dimensions of land degradation – status, trends and drivers – resulting in a better understanding of the spatial relationships between the causes and processes involved. The combination of biophysical status with trends resulted in a map showing areas at risk: areas with a negative trend and a low status and areas with a high negative trend and a high status. Combining trend with drivers produced a map that differentiates between human-induced land degradation, deterioration, and stable or improving biophysical conditions. Human-induced land degradation refers to a negative trend, which is most likely caused by human activity. Deterioration refers to a negative trend presumably caused by natural phenomena, but that may also have anthropogenic origins where status is low. This will be further discussed in Section 3.4.2.

2.2 Harmonization

The acquired geospatial information varied in format (vector and raster data) and spatial resolution (30 arc seconds to 30 arc minutes). Prior to the analysis, all data layers were harmonized to the GAEZ v4 format: GeoTIFF raster with 4 320 pixels width, 2 160 pixels height and pixel size of 0.0833 degrees (five arc minutes, approximately 9 by 9 km^2 at the equator, and 6 by 6 km^2 at the Arctic Circle). The coordinate reference system was set to EPSG: 4326 - WGS 84 - geographic with extent xmin = -180, xmax = 180, ymin = -90 and ymax = 90. The origin was x= - 180 and y = 90. To allow for comparison between layers and to perform calculations, units and ranges were standardized. Normalization with a stretch from 0 to 10 was applied to the status and driver input layers. Row standardization is a normalization technique that can cope with both negative and positive values and was applied to the trend layers. This resulted in rasters with values ranging from -1 to 1. When the frequency distribution of a data set was very skewed, high or low values had a disproportionate influence, blurring differences in the middle ranges. To dampen this effect, the distribution was trimmed and extreme values were replaced by a chosen percentile. Low and high quantiles ranging from the first to fifth percentile and from the 95th to 99th percentile, respectively, were used for normalization. The percentile was selected on the basis of the histogram of each layer. Figure 1 shows an example of the normalization.

Figure 1. Normalization of global soil organic carbon layer

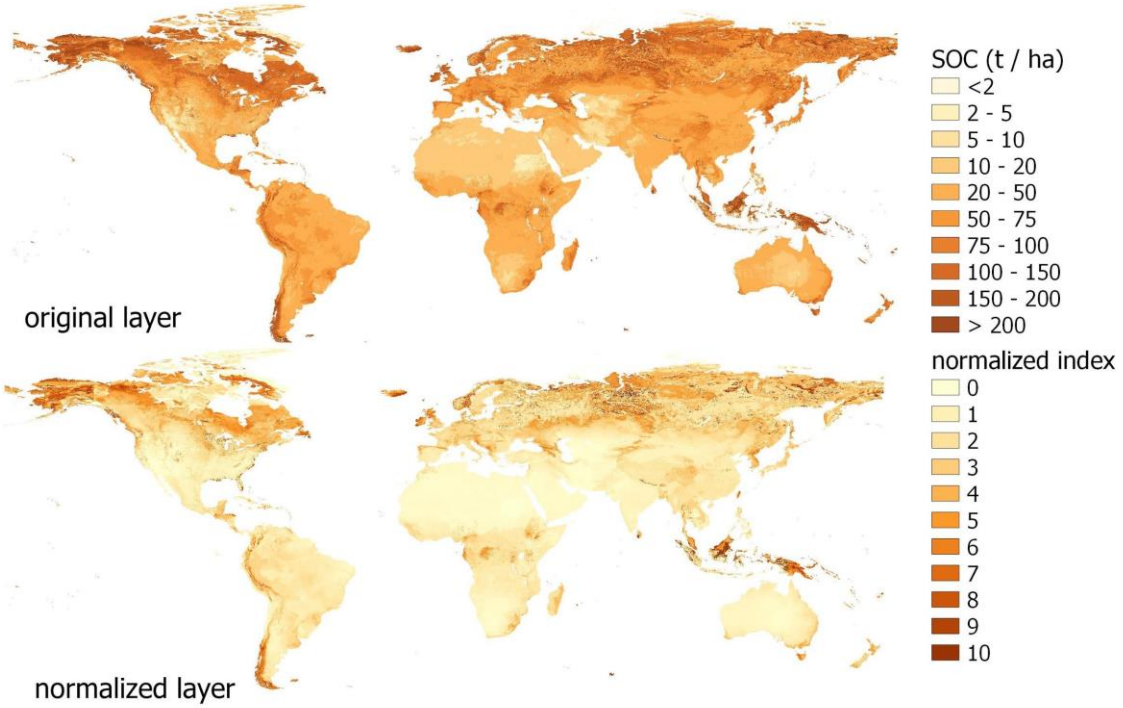

Source: FAO & ITPS). 2018. *Global Soil Organic Carbon Map (GSOCmap)*. Technical report. Rome, FAO. Available at https://storage.googleapis.com/fao-maps-catalog-data/geonetwork/gsoc/GSOCmap/GSOCmap1.5.0.tif. Modified to comply with UN. 2020. Map of the World. https://www.un.org/geospatial/file/3420

2.3 Biophysical status

Overall status was determined using nine input layers that reflect present biophysical conditions. For information about the resolution and availability of the layers, see Annex I. Low values correspond to a low status and high values correspond to a high status. For example, a high erosion rate implies a low status and during the normalization, the values were reversed so that low index values correspond to high erosion rates. A brief description of the nine input layers follows:

1. Availability of soil nutrients: nutrient availability and nutrient retention capacity from GAEZ v4 (Fischer *et al.,* 2021) were combined.

2. Soil carbon content: soil organic carbon stock from 0 to 30 cm (FAO and ITPS 2018).

3. Water erosion (Guerra *et al.*, 2020): mean erosion rate between 2001 and 2013, calculated with an adapted universal soil loss equation and remote sensing models.

4. Wind erosion: spatial and temporal occurrence of anthropogenic dust sources (based on Ginoux *et al.*, 2012). Dust sources were mapped based on Moderate Resolution Imaging Spectroradiometer (MODIS) Deep Blue estimates of dust optical depth in conjunction with other data sets, including land use. Dust sources were ascribed to natural and anthropogenic (primarily agricultural) origins, their respective contributions to emissions were calculated and extensively compared against literature (Ginoux *et al.*, 2012).

5. Groundwater recharge: groundwater recharge classes per aquifer type (Richts *et al.*, 2008).

6. Scarcity, Flexibility and Variability (SFV) Water stress (Qin *et al.*, 2019): The SFV water stress index integrates the share of runoff being consumed (scarcity), the share of consumption in these inflexible categories (flexibility), and the historical variability of runoff weighted by storage capacity (variability) for major river basins (GRDC, 2020).

7. Native species richness (Ellis *et al.*, 2012): The number of native vascular plant species was estimated using the species richness model of Kreft and Jetz (2007). This model is based on empirical statistical relationships between environment (potential evapotranspiration, number of wet days per year, topographic and habitat heterogeneity, and three-dimensional vegetation complexity) and species richness patterns obtained from datasets documenting the number of native species in 1 032 geographic regions worldwide.

8. Above ground biomass: Forest biomass was taken from European Space Agency's Globbiomass project (Santoro *et al.*, 2018). To calculate biomass for shrubs, grasslands and herbaceous vegetation/wetlands, values were derived from literature (Junk and Piedade, 1993; Penman *et al.*, 2003; Carrillo *et al.*, 2006; Peregon *et al.*, 2008; Hamdan *et al.*, 2010; Truus, 2011; Lou *et al.*, 2016; Estrada and Soares, 2017; Lumbierres *et al.*, 2017; Conti *et al.*, 2019; Han *et al.*, 2019; Miller *et al.*, 2019) for each IPCC climate zone and subsequently multiplied by the percentage cover of the corresponding GLC-SHARE layer (Latham *et al.*, 2014).

9. GLC-SHARE artificial cover layer: The layer is composed of any type of area with a predominant artificial surface. Any urban or related feature is included. The class also includes industrial areas, waste dump deposits and extraction sites (Latham *et al.*, 2014).

To calculate the overall biophysical status index, the normalized layers were added and divided by the number of layers. The index was corrected for areas that were not covered by all layers. The water stress layer refers to the main river basins; many coastal zones or inland areas with internal drainage are not covered. The layer has relatively high values and its absence causes sharp drops or rises in status, which are clearly visible on the overall status map. To reduce this border effect, the layer is down-weighted by 0.5. The classification for the status was based on the quantiles of the index value (see Table 2). Class 1 consists of values between minimum and 1st quantile; Class 2 comprises values between 1st quantile and median; Class 3 consists of values between median and 3rd quantile and Class 4 comprises the values from 3rd quantile to maximum.

Table 2. Reclassification of the overall biophysical index

Class	Description	Quantiles	Index
1	Very low status	1st Quantile	1 - 3.8
2	Low status	Median	3.8 - 4.4
3	Moderate status	3rd Quantile	4.4 - 4.9
4	High status	Maximum	4.9 - 8.2

2.4 Trends

Overall trend was determined by seven input layers showing changes in soil, water, vegetation and population density. For information about the resolution and availability of the layers, see Annex I. Negative change can imply decline or improvement, depending on the variable. A negative change in soil erosion rate implies that soil erosion is diminishing and is regarded as improvement. A positive change in water stress implies that water stress is increasing which is regarded as decline. Values around zero mean that no change took place. A brief description of the seven trend layers follows:

1. Soil erosion rate change, 2000 – 2012 (Borrelli *et al.*, 2017).

2. Soil protection change, 2001 – 2013: Soil erosion protection is defined as the amount of soil that is prevented from erosion by water through the influence and erosion mitigation capacity of available vegetation (Guerra *et al.*, 2020).

3. Fresh water change: changes in terrestrial water storage (groundwater, soil moisture, surface waters, snow and ice), 2002 – 2016 (Rodel *et al.*, 2018).

4. SFV Water stress change (based on Qin *et al.*, 2019 and GRDC, 2020): the difference between the water stress index in 2016 and 1980.

5. Change in land productivity 1999 – 2013 (Cherlet *et al.*, 2018): The annual growing season accumulation of the above ground biomass production is a proxy for net primary productivity (NPP). The dynamics, observed by satellite and derived from phenological analyses of a 15-year time series, point to long-term alterations of the health and productive capacity of the land.

6. Forest biomass change: Forest biomass with reference year 2010 by Santoro *et al.* (2018) was compared with the global biomass map compiled by Ruesch and Gibbs (2008) with reference year 2000.

7. Population density change (based on CIESIN, 2018): Maps of population density in 2020 and 2000 were prepared and the difference was calculated.

The overall trend index was calculated by summing the normalized input layers divided by the number of layers. No weighting was applied and the index was corrected for areas that were not covered by all layers. The classification for the trend was based on quantiles of the index value (see Table 3). Class 1 consists of values between minimum and 1st quantile; Class 2 comprises values between 1st quantile and median; Class 3 consists of values between median and 3rd quantile and Class 4 comprises the values from 3rd quantile to maximum.

Table 3. Reclassification of the overall trend index

Class	Description	Quantiles	Index
1	Strong to moderate decline	1st Quantile	-1 to -0.116
2	Light decline	Median	-0.116 to -0.011
3	Stable	3rd Quantile	-0.011 to 0.064
4	Improvement	Maximum	0.064 to 0.535

2.5 Drivers

Six input layers of direct anthropogenic drivers were used to calculate the driver index. For information about the resolution and availability of the layers, see Annex I. Low values correspond with low pressure by drivers and high values correspond to high pressure. A brief description of the six drivers layers follows:

1. Agricultural expansion: The global land cover data from 2000 (EC/JRC, 2003) was compared with the crop cover layer of GLC-SHARE with reference year 2014 (Latham *et al.*, 2014). Areas that were not cultivated in 2000 and had a crop cover larger than 10 percent in 2014, or areas with a mosaic of crops and other vegetation in 2000 that had a crop cover larger than 20 percent in 2014 were classified as expansion. The percentage of crop cover in 2014 was taken as the measure of pressure.

2. Deforestation: The global forest change (GFC) data (Hansen *et al.,* 2013) was combined with the World Atlas of Desertification (WAD) forest loss from Cherlet *et al.*, (2018). Comparison of both layers with the source layer of 30 by 30 m^2 (Hansen *et al.,* 2013) showed that the GFC layer corresponded roughly with 60 percent deforestation and that the WAD layer corresponded approximately with 20 percent deforestation. The combined layer was reclassified by giving the area covered by GFC a value of six and the remaining area covered by WAD a value of two (on a scale of zero to ten).

3. Fire (based on Archibald *et al.*, 2013): Fire return interval was combined with fire size. The maximum interval was set at 20 years and the maximum size was set at 500 km^2. Subsequently the layers were normalized, multiplied and normalized again.

4. Grazing density: Global livestock distribution data (Gilbert *et al.*, 2018) with reference year 2010 were used to calculate tropical livestock unit (TLU) per livestock production system (LPS) as described by Robinson *et al.* (2011). In accordance with FAO (2013), TLU densities per LPS were calculate for separate regions (New Zealand/Australia, West Europe, East Europe/Central Asia, North America, Latin America and the Caribbean, East Asia, South Asia, sub-Saharan Africa, and North Africa and the Middle East). TLU density per LPS per region was normalized and merged for the region. Subsequently, all regions were merged.

5. Accessibility (Weiss *et al.*, 2018): Global map of travel time to cities to assess inequality in 2015.

6. Ratio invasive/native species (Ellis *et al.*, 2012): Invasive species are modelled applying a global statistical relationship with native species (Lonsdale, 1999), based on 177 flora worldwide and adjusted according to the average proportions of invasive plants in Lonsdale's eight coarse biomes.

Table 4. Reclassification of the cumulative pressure by direct anthropogenic drivers

Class	Description	Quantiles	Index
1	Very low pressure	1st Quantile	0 - 3.8
2	Low pressure	Median	3.8 - 6.6
3	Moderate pressure	3rd Quantile	6.6 - 11.5
4	High pressure	Maximum	11.5 - 42

To calculate the cumulative pressure of the drivers, the layers were added. The values of the resulting layer varied from zero to 42. For subsequent analysis, the layer was reclassified on the basis of the quantiles of the pressure index (see Table 4). Class 1 consists of values between minimum and 1st quantile; Class 2 comprises values between 1st quantile and median; Class 3 consists of values between median and 3rd quantile and Class 4 comprises the values from 3rd quantile to maximum.

The main driver was determined by assessing – for each pixel – which driver had the highest value. Accessibility dominated the other drivers by far in regions with low to moderate cumulative pressure and was weighted down with 0.5. The invasive/native species ratio layer dominated large parts of North America, Europe and Siberia and was weighted down with 0.25.

2.6 Areas at risk and human-induced land degradation

The combination of overall biophysical status with overall trend gave an overview of areas at risk. These were defined as large contiguous areas of low status and subject to decline, possibly interspersed with areas of strong decline and high status. Stable or improving areas are currently not at risk, regardless of status. The integration of both layers resulted in 16 possible combinations, which were reduced to six classes to improve the readability of the map (see Table 5).

The combination of trend with drivers and status enabled the production of a land degradation map. A negative trend coinciding with high pressure was classified as human-induced degradation. High pressure was defined as cumulative pressure values above the third quantile (see Table 6). A negative trend coinciding with low and moderate pressure is likely to be of natural origin but, in areas with low status, the decline may also be caused by human activity or a combination of both, and is classified as deterioration. This will be further discussed in Section 3.5.

A hot spot analysis was conducted on the combined driver and trend data set. The strong and light human induced land degradation classes were selected to identify where human induced land degradation is concentrated in large contiguous areas. The analysis used the Getis-Ord Gi* statistic, which calculates z-scores and p-values to test whether a variable is clustered spatially. The classification of a statistically-significant hot spot requires that the variable has z-scores higher than 1.96 and is surrounded by other high z-scores, all with p-values lower than 0.05 were identified.

Table 5. Biophysical status and trend combined[1]

Trend	Status 1, 2 & 3	Status 4
1	Low status and strong decline: at risk	High status and strong decline: at risk
2	Low status and light decline: at risk	High status and light decline
3 & 4	Low status and stable or improvement	High status and stable or improvement

[1] The colours in Table 5 correspond with those used in the map in Section 3.4.1.

Table 6. Land degradation classes[2]

Trend	Pressure 1, 2 & 3	4
1	Strong deterioration under low to moderate pressure	Strong human-induced land degradation
2	Light deterioration under low to moderate pressure	Light human-induced land degradation
3 & 4	Stable or improvement under low to moderate pressure	Stable or improvement under high pressure: high resilience

2.7 Multidimensional degradation analysis for global land cover

The land cover dataset of the global agro-ecological zones (GAEZ) produced by Fischer *et al.* (2021) was combined with the land degradation map to calculate the area of seven aggregated land cover classes (rainfed cropland, irrigated cropland, grassland, forestland, shrubs, herbaceous vegetation and sparse vegetation) and the aggregated protected area class for each SOLAW region and country groups (high-, upper middle-, lower middle- and low-income countries, the low-income and food-deficit countries and the least-developed country group). The layer with contiguous areas of concentrated human induced land degradation was combined with the irrigated cropland layer.

A hot spot analysis was conducted on the combined status and trend data set. The areas at risk classes were selected and combined with the dominant land cover classes of crops, grassland and forest.

2.8 Caveats and limitations

Inherent in a global environmental study are the limitations imposed by the availability of data. The baseline of the trend analysis should represent pre-degradation conditions but, as most global geospatial data sets do not date back further than the 1980s, when remote sensing was first introduced in environmental science, the full magnitude of the decline is not always known. Ideally, the input layers should have the same resolution, cover all aspects of the corresponding dimension, represent the same time period in case of trend, and be equally distributed over the three dimensions, status, trends and drivers. In this study, however, some layers had a significantly lower resolution (native and invasive species, fire, change in available freshwater, groundwater) or higher resolution (deforestation), were significantly older (groundwater, plant native and invasive species, fire, wind erosion) or covered much longer time periods (water stress change). Also, the input layers were not equally distributed over the dimensions.

The advantage of using readily available datasets from high-profile journals was that their quality was guaranteed by the peer review process. The disadvantage was that not all the necessary information was available so that some factors were missing from the analysis or remained underexposed. Agricultural management was only represented by grazing

[2] The colours of Table 6 correspond with the map in Section 3.4.2.

density and the impact of industrial development and pollution was not addressed at all. This will be discussed further in Sections 3.4.3 and 4.2.

Climate change was not directly included in this study due to its complexity and uncertainties around positive and negative feedback loops between land degradation and climate change. Climate change can be a direct or an indirect driver and is both natural and human-induced (Olsson *et al.*, 2019). Despite the complex spatial impact of climate change on land degradation and vice versa, there is general agreement that human-induced climate change is directly driving an increase in coastal erosion, the accelerated thawing of permafrost and increased burning (Olsson *et al.,* 2019). There are no global datasets available for coastal erosion or thawing of permafrost, but the return interval and extension of fire were included in this study. Climate change was also addressed indirectly by layers concerned with change in water stress, change in available freshwater, change in land productivity and invasive species.

Classification creates sharp boundaries, which poorly reflect the continuous nature of most variables. Labelling classes offer a false certainty about the nature of a value. Stratification – classification based on scientifically established, variable-specific thresholds per region – would have greatly improved the assessment but, unfortunately, this information was not available for most variables at the global level. The second-best option was to classify variables with the help of simple statistics such as minimum, first quantile, median, third quantile and maximum value. The advantage of this method is its flexibility: a modification in the input layers did not lead to dramatic changes in the output because the classes were automatically adjusted and relative differences remained largely intact. For example, labelling a range of index values 'low' merely indicated that this range had lower values than the class labelled 'moderate.' It did not give information about the absolute value nor about its significance in the local context; this worked reasonably well for the calculation of a status index at the global level but less well for trend and drivers. This will be further discussed in Sections 3.4.3 and 4.2.

The extreme values in skewed distributions were removed during the normalization process by setting percentiles. Although the cut-off values did not exceed 5 percent and were chosen on the basis of the histogram of each layer, the decision as to which percentile to use was subjective. This will be discussed further in Section 4.2.

3. Integration of three land degradation dimensions

3.1 Biophysical status

Very low and low values for status were found in drylands, cold zones (with a potential evapotranspiration – PET – of less than 400 mm/year) and on steep terrain and appear to be related directly to climate and geomorphology (see Figure 2). Most of the land with a moderate biophysical status was also situated in arid to sub-humid, cold or mountainous environments. Flat and humid areas with a moderate status were located throughout Europe, West Africa, the northern and southern parts of the Congo basin, the Parana basin in southeast Brazil, Paraguay and north Argentina, and the southwest coast of the United States of America. A high biophysical status was mostly found in the remaining flat and humid regions as well as in the dry Gran Chaco in the southeast of the Plurinational State of Bolivia and northwest Paraguay. Mountainous areas with a high status were situated in the upper Amazon basin at the foot slopes of the Andes, the western Canadian Rockies, the south coast of Quebec, Japan's northernmost main island Hokkaido, the mountain ranges in Borneo and New Guinea, and the Australian Alps. The highest biophysical status areas were found in the lowland rainforests of the Amazon basin and the Guianas, the Choco region along the northern coast of Ecuador and the Pacific coast of Colombia and eastern Panama, from the southern Gulf of Guinea to the Congo basin, and in the southern part of the Malay Peninsula, on Sumatra, Borneo and New Guinea.

3.2 Trend

3.2.1 Decline

In general, an overall decline in status was the result of various combined negative trends in an affected area. The combinations of input layers that were responsible for negative trends are summarized per region in Annex II and described below.

Figure 2. Overall biophysical status

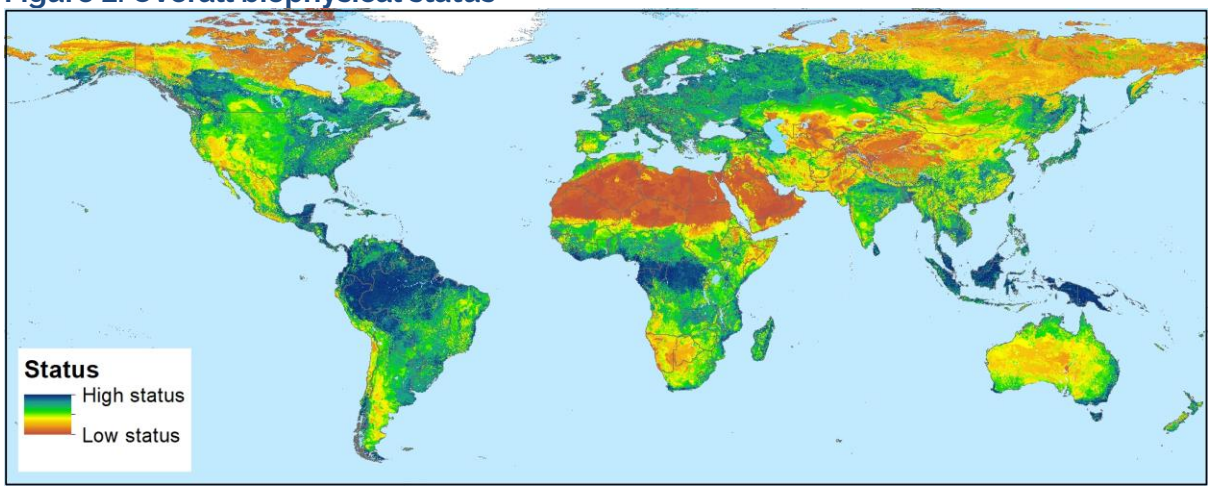

Source: United Nations Geospatial. 2020. Map geodata https://www.un.org/geospatial/file/3420. New York, USA, United Nations, modified by the author.
Notes: Final boundary between the Sudan and South Sudan has not yet been determined. Dotted line represents approximately the Line of Control in Jammu and Kashmir agreed upon by India and Pakistan. The final status of Jammu and Kashmir has not yet been agreed upon by the parties.

The trend analysis revealed that even the few remaining regions with large, contiguous tropical rainforests are subject to decline (see Figure 3). Only some areas in the core of the Amazon, the eastern part of the Congo basin and isolated patches in Borneo, were stable or improving. For most rainforests, decreasing forest biomass and increasing population resulted in a negative trend but locally, decreasing soil protection and increasing erosion rates also contributed.

In most affected regions, decreasing freshwater availability was a recurring contributor to overall decline. Around the Hudson Bay in Canada and from southern Alaska to southwest Yukon, it was the sole responsible factor while in British Columbia, a reduction in land productivity and soil protection also contributed. A reduction in available freshwater and land productivity were responsible for affected areas in northern Alberta, northern Saskatchewan and the Northwest Territories. In western Washington in the United States of America, a combination of decreasing forest biomass and increasing population density was responsible for a negative trend. In California, apart from a decrease in freshwater availability, higher population density and less soil protection were contributing to the negative trend. In neighbouring Nevada, decreasing freshwater is the main issue, while in Texas various combinations of all input layers (with the exception of erosion rate) were responsible for the negative trend. In the southeast, a higher population density and a lower forest biomass and soil protection contributed to overall decline. The Sierra Madre Occidental in Mexico was subject to a reduction in available freshwater, forest biomass and soil protection. The Yucatan peninsula and the Caribbean coast of Central America experienced decreasing forest biomass and soil protection and increasing population density and soil erosion rates.

In Iceland, a strong reduction in freshwater availability was solely responsible for the negative trend, while in Spain, increased SFV water stress and population density were responsible. The vast area covering eastern Ukraine, southern Russia and western Kazakhstan was mainly affected by decreasing freshwater availability but also by lower land productivity and soil protection. The affected areas in Siberia were also the result of reduced freshwater availability and decreased land productivity.

Affected areas in West and South Asia were subject to decreasing freshwater, increasing water stress and population density. In southern India, especially along the southeast coast, an additional factor was a strong reduction in forest biomass. The mountain ranges of Hindu Kush, Pamirs and Tien Shan were exposed to decreasing freshwater and severe water stress, and the Karakoram and eastern Kunlun Shan ranges were exposed to population density increases as well. In south and east Tibet, an additional factor was decreasing soil protection. A large area stretching from the Loess Plateau in north-central China to the Bohai Sea region faced a combination of population density increase, water stress increase, freshwater availability decrease and soil protection decrease. The coastal zone of southeastern China was exposed to increased population density, soil erosion and decreased forest biomass. In Southeast Asia, increased population density and soil erosion, and decreased soil protection and freshwater availability were common issues. The mainland also coped with increased water stress and the islands experienced decreasing forest biomass.

Figure 3. Overall trends

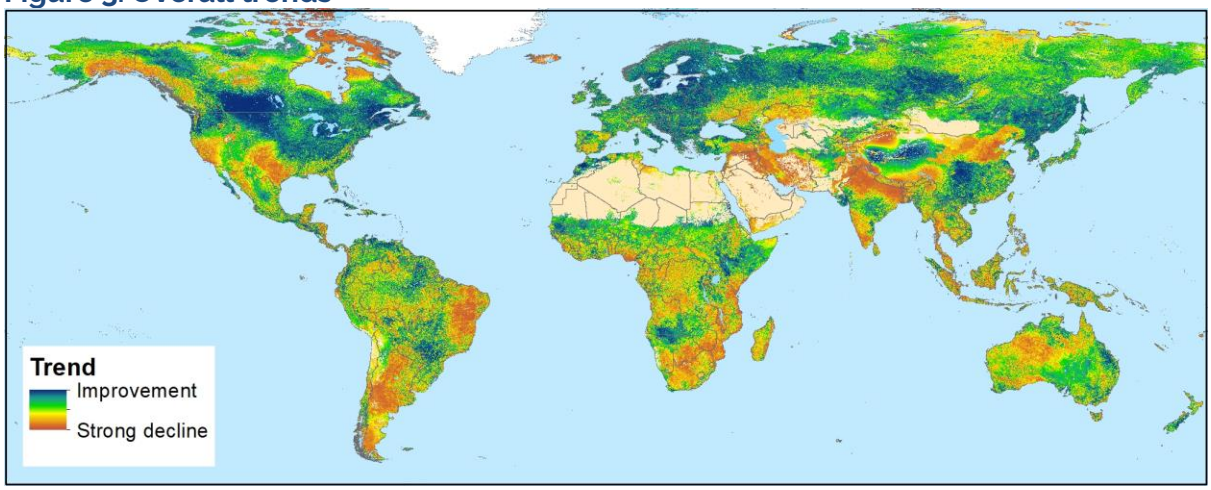

Source: United Nations Geospatial. 2020. Map geodata https://www.un.org/geospatial/file/3420. New York, USA, United Nations, modified by the author.

Notes: Final boundary between the Sudan and South Sudan has not yet been determined. Dotted line represents approximately the Line of Control in Jammu and Kashmir agreed upon by India and Pakistan. The final status of Jammu and Kashmir has not yet been agreed upon by the parties.

All affected areas in Australia faced decreasing land productivity and soil erosion protection. The western half of Australia has also seen a decrease in freshwater, while in the southeast increased SFV water stress was an additional issue.

The northern Nile valley was subject to SFV water stress, decreasing freshwater and increasing population density. In Ethiopia, diminishing soil protection, higher erosion rates and more water stress led to a strong decline in status. In southeast and East Africa, a decrease in available freshwater and rising population density were the main contributors to a decline in status. Locally, in coastal regions, strong decreasing forest biomass contributed as well to the overall negative trend. Madagascar faced increasing population density and decreasing soil protection, freshwater availability and, along the east coast, a reduction in forest biomass. In southern Africa, greater water stress, and less soil protection and land productivity and a slight decrease in freshwater caused a negative trend. In West Africa, the combination of an increase in population density and a decrease in forest biomass and locally soil protection resulted in a decline in status.

A vast area in east Brazil was affected by decreasing freshwater and soil protection, and increased SFV water stress and soil erosion. In the Chaco region of north Argentina and western Paraguay, decreasing land productivity, forest biomass and soil protection and increasing water stress resulted in a negative trend. The decrease in freshwater availability was less prominent. At the northern border of the Chaco, east of Santa Cruz in the Plurinational State of Bolivia, changes in population density, soil protection, soil erosion rates and land productivity caused a decline in status. In central and south Argentina, a decrease in freshwater availability was the main responsible factor with decreasing soil protection in central Argentina and increasing soil erosion rates and population density contributing as well.

3.2.2 Stable or improvement

Extensive stable or improving areas were found in the Mackenzie mountains around the border region of Yukon and Northwest Territories and in the southern prairies and the

eastern taiga of Canada; the northern and eastern prairies, and the Great Lakes temperate forests of the United States of America; Eastern Europe, the Eurasian taiga and the eastern part of the Eurasian steppe (see Figure 3). Large parts of the Tibetan plateau, Manchuria, the Democratic People's Republic of Korea, the Republic of Korea and temperate southeast China (Guizhou, Sichuan, Yunnan, Hunan, Hubei, Henan and Guanxi) are stable or improving and the northeastern part of the Deccan plateau in India is improving as well.

In the eastern and southern parts of the Australian interior, a large stable area is situated. In Africa, most of Morocco and the southern Sahel zone showed stable and improving conditions, as well as the lowlands of Ethiopia, south Somalia and north Kenia, and the border region of Angola, Zambia, Botswana and Namibia. The eastern slopes of the central Andes and parts of the northern Andes in north Peru, Ecuador and south Colombia had a stable or improving status, as did large areas in the north of the Bolivarian Republic of Venezuela. A zone stretching from south Suriname to the Amazon River and west towards Manaus also showed stable or improving conditions.

3.3 Drivers of land degradation

At the global level, there are a few regions where many drivers converge, resulting in vast continuous areas where the pressure on soil, water and vegetation resources is high (see Figure 4). These regions include the East Coast of the United States of America, including the Great Lakes area and the Mexican Gulf Coast states; Western, Central and Eastern Europe, and the adjacent Volga basin in the Russian Federation; East Pakistan, India and Bangladesh; central east China, the Democratic People's Republic of Korea, the Republic of Korea and Japan. For information about the combination of drivers that act on the regions, please see Annex III.

Figure 4. The cumulative effect of direct human drivers of land degradation

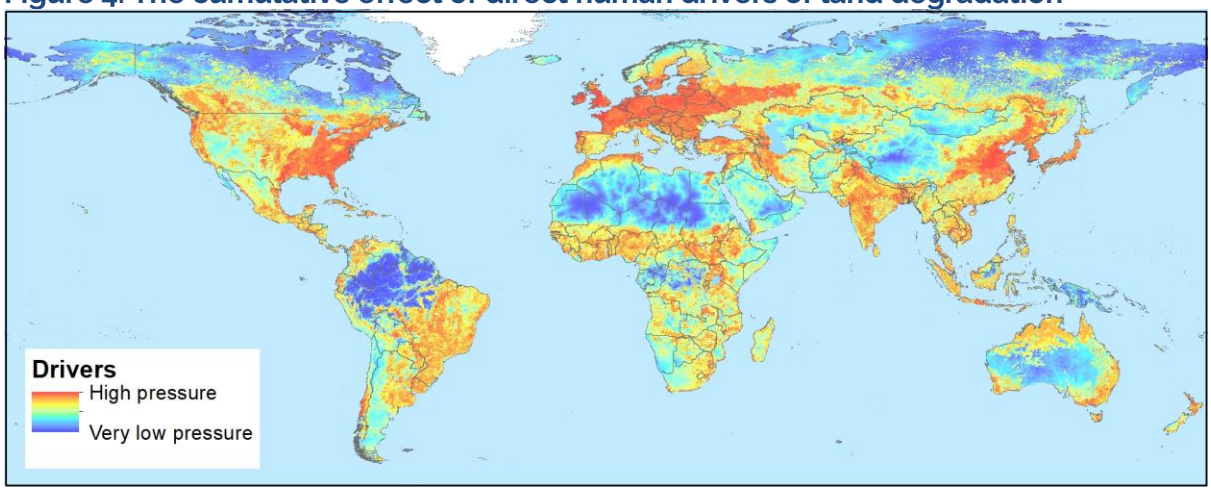

Source: United Nations Geospatial. 2020. Map geodata https://www.un.org/geospatial/file/3420. New York, USA, United Nations, modified by the author.

Notes: Final boundary between the Sudan and South Sudan has not yet been determined. Dotted line represents approximately the Line of Control in Jammu and Kashmir agreed upon by India and Pakistan. The final status of Jammu and Kashmir has not yet been agreed upon by the parties.

Patches with moderate to high pressure were found in many regions; these were frequently interspersed with low to very low pressure. The affected regions are British Columbia and the prairies of southern Alberta and Saskatchewan, Canada; the West Coast and a stretch of the Great Plains from southwest Nebraska to northwest Texas in the United States of America; the area that covers both the Gulf and Pacific coast and the southern altiplano of Mexico, and the Pacific coast of Central America; the greater Antilles in the Caribbean; the Eurasian steppe of northern Kazakhstan; western Yemen; Northern West Asia; the coastal zone of southeast China and the mainland of Southeast Asia; the Philippines and Java.

In the north, southwest and southeast of Australia, and in the North Island of New Zealand, patches of high pressure interspersed with areas exposed to moderate to low pressures were found. A similar pattern occurred in the Maghreb; the northern Nile Valley; the upper Nile basin stretching from the Ethiopian highlands via southern Sudan and east South Sudan to Uganda and the shores of Lake Victoria; Southern Africa; Nigeria and the adjacent West African coast. In Brazil, there were several patches with high pressure in the proximity of the Bolivian, Paraguayan and Argentine borders, in the eastern part of the Parana basin, the Tocantins basin, the western Sao Francisco basin, and along the east and south Atlantic coast, which continues into the pampas of Uruguay and the Buenos Aires province of Argentina; South central Chile between the city of Santiago and island of Chiloé; the Peruvian Andean highlands; the region extending from the Ecuadorian coastal plain through the inter-Andean valley and the Cauca and Magdalena valleys in Colombia to the Caribbean coast and los Llanos in the western fringe of the Orinoco basin of Colombia and the Bolivarian Republic of Venezuela.

Figure 5. The global distribution of the dominant direct human driver per area

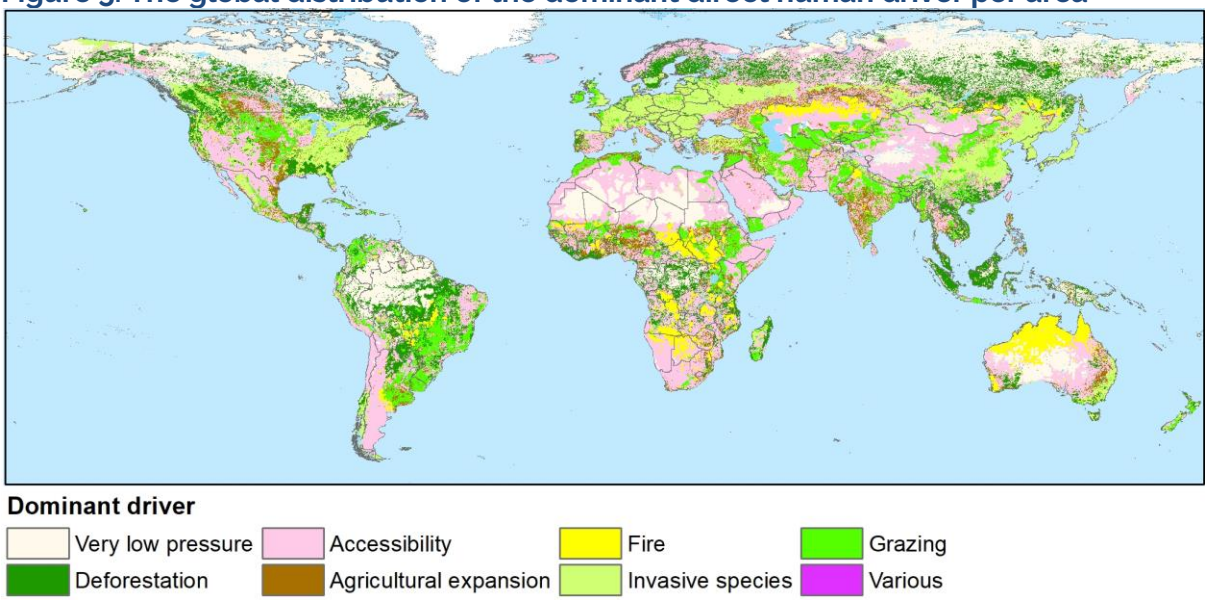

Source: United Nations Geospatial. 2020. Map geodata https://www.un.org/geospatial/file/3420. New York, USA, United Nations, modified by the author.

Notes: Final boundary between the Sudan and South Sudan has not yet been determined. Dotted line represents approximately the Line of Control in Jammu and Kashmir agreed upon by India and Pakistan. The final status of Jammu and Kashmir has not yet been agreed upon by the parties.

Figure 6. Regions at risk: overall biophysical status combined with overall trends

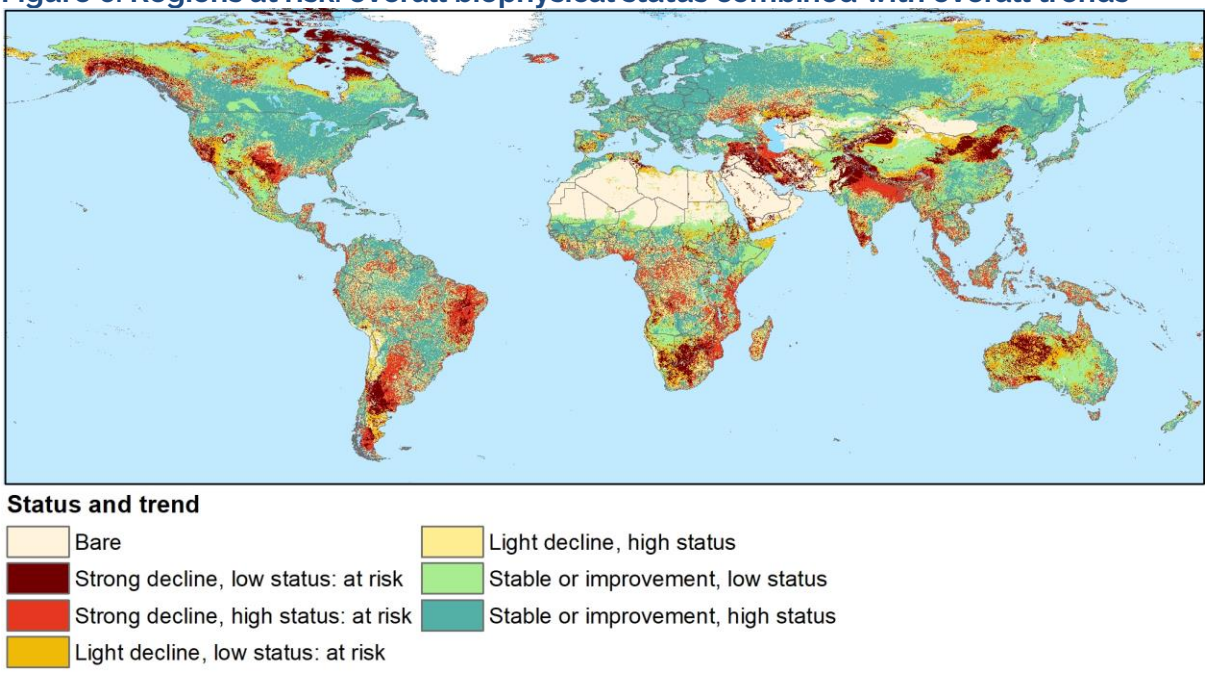

Source: United Nations Geospatial. 2020. Map geodata https://www.un.org/geospatial/file/3420. New York, USA, United Nations, modified by the author.

Notes: Final boundary between the Sudan and South Sudan has not yet been determined. Dotted line represents approximately the Line of Control in Jammu and Kashmir agreed upon by India and Pakistan. The final status of Jammu and Kashmir has not yet been agreed upon by the parties.

The global distribution of the main driver is shown in Figure 5. The main driver is dominant relative to the other drivers in terms of pressure but is not necessarily responsible for human-induced land degradation since low and moderate pressure were included in the analysis as well. Grazing and agricultural expansion were common in large parts of the United States of America, while invasive species and deforestation dominated in Alaska, northern Canada, northern Europe and Siberia. Invasive species also dominated in Europe. In the Asian steppe, the most frequent drivers were fire and grazing, and in south and southeast Asia population density and deforestation were common. Australia was exposed to fire and New Zealand was subject to high grazing densities. In Africa, fire and grazing were common, and in South America grazing and deforestation dominated.

3.4 Integration of status, trends and drivers

3.4.1 Areas at risk

According to Rodell *et al.* (2018), global warming causing ice sheet loss and melting glaciers was responsible for a significant reduction in available freshwater in the Eastern Arctic region of Canada and the stretch from southern Alaska to southwest Yukon (see Figure 6). Groundwater depletion and drought have reduced freshwater availability in California and adjacent Nevada (Rodell *et al.*, 2018). In Texas, soil, water and vegetation resources were in sharp decline, due to a combination of drought, grazing, population pressure and expanding agriculture (see Figure 5). Soil protection decline, high soil erosion rates and SFV water stress were responsible for fragile conditions in the Sierra Madre Occidental in Mexico.

Parts of Spain faced increasing SFV water stress, and groundwater depletion. Groundwater depletion and drought in west Kazakhstan have led to a decline of the Caspian and Aral Seas. Large areas in West Asia were at risk because of severe groundwater depletion, drought and population increase. East Pakistan and northern India were exposed to groundwater depletion and population pressure, whereas in southeast India, water stress and agricultural expansion were major issues. The semi-arid area from the Loess Plateau in north-central China to the Bohai Sea region experienced severe groundwater depletion and population pressure. Western Australia received less rainfall, in combination with a decline in land productivity and large frequent fires.

The eastern Maghreb was exposed to agricultural expansion and decreasing freshwater availability. The northern Nile Valley was subject to high intensity grazing, population pressure and increasing water stress. In the Ethiopian highlands, soil erosion caused by intensive grazing and agricultural expansion were major issues. Southern Sudan coped with agricultural expansion and increasing water stress. The western part of South Sudan was affected by large and recurrent fires and was also subject to massive forest biomass loss and increasing SFV water stress. Southern Africa faced increasing water stress and a decline in land productivity. Eastern Brazil was affected by a recent drought, which caused increased water stress and decreased land productivity. The same effects were found in central Argentina, where precipitation was decreasing and large areas were burned.

Stable or improving regions with low biophysical status were located in the western Arctic zones of North America and Eurasia and at the edges of the great deserts, such as the Sahara (the Sahel), the Karakum in Central Asia, the Gobi in East Asia and the Kalahari in southwest Africa. The arid and semi-arid regions of the Taklamakan desert, the Tibetan plain, southeast Australia and the Horn of Africa exhibited low resistance as well.

Stable or improving regions with high biophysical status were found throughout southern Canada, and the northern and central east part of the United States of America. The stable or improving regions stretching from central and southeast Europe to the Eurasian taiga, and from east Mongolia to Manchuria had a high biophysical status as well.

3.4.2 Human-induced land degradation

At the global level, three regions were severely affected by human-induced land degradation over large contiguous areas: the arc in northern West Asia, stretching from Israel to southeast Türkiye into Mesopotamia and western Islamic Republic of Iran; the Indo-Gangetic plain south of the Himalaya on the Indian subcontinent; and north China, from the Loess Plateau to the Yellow River Basin and the Bohai Sea region (see Figure 7). However, almost all inhabited parts of the world were subject to some form of human-induced land degradation and 52 degrading regions have been identified using an optimized hotspot analysis (see Section 2.6). Grazing occurred in 75% of the identified regions, followed by accessibility (71%) and agricultural expansion (64%). The affected regions and the corresponding drivers are presented in Annex IV.

Figure 7. Global distribution of human-induced land degradation: overall trend combined with the cumulative pressure by direct human drivers

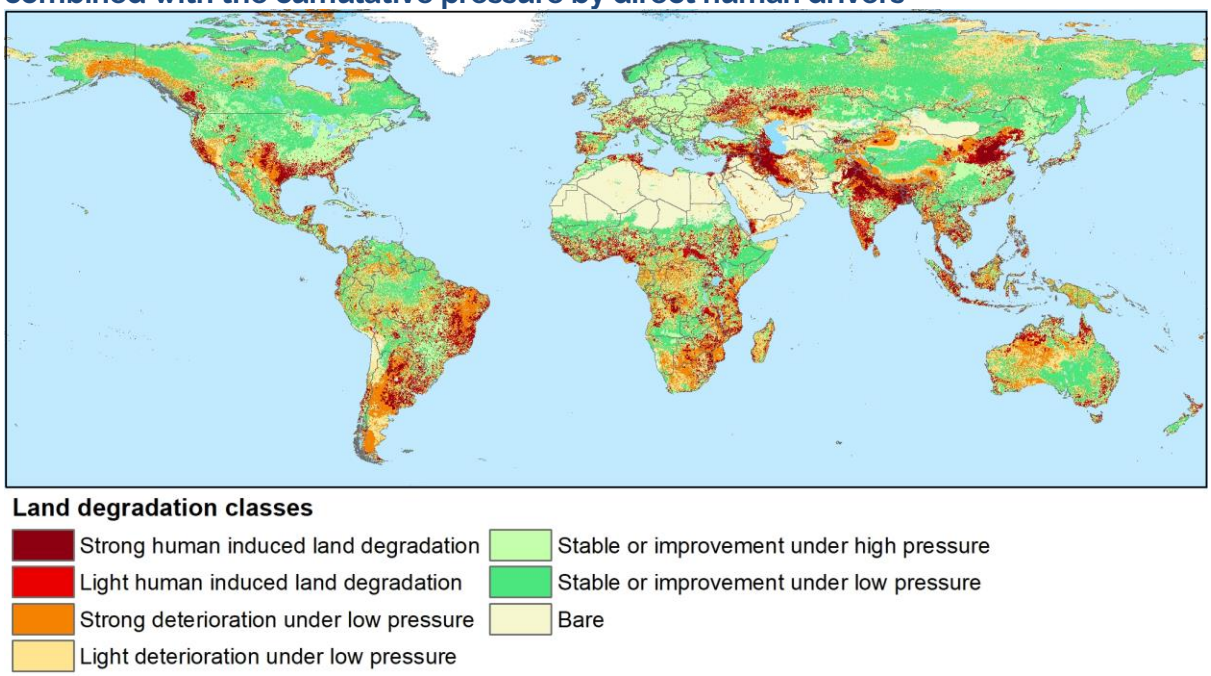

Source: United Nations Geospatial. 2020. Map geodata https://www.un.org/geospatial/file/3420. New York, USA, United Nations, modified by the author.

Notes: Final boundary between the Sudan and South Sudan has not yet been determined. Dotted line represents approximately the Line of Control in Jammu and Kashmir agreed upon by India and Pakistan. The final status of Jammu and Kashmir has not yet been agreed upon by the parties.

Globally, areas affected by human-induced land degradation covered 1 660 Mha (million hectares), of which 850 Mha is moderately to severely degraded and 810 Mha is slightly degraded (see Table 7). Degraded areas were fairly evenly distributed over drylands and humid areas, although humid areas had a higher share of light degradation. Human-induced land degradation occurred in 11 percent of the drylands and in 15 percent of the humid areas.

A fifth of the global human-induced degraded land can be found in sub-Saharan Africa, followed by South America with 17 percent (see Table 8). North America is about five times the size of South Asia but both contribute 11 percent to global degradation. In relative terms, South Asia was the most affected region, with 41 percent of its area suffering from man-made degradation, of which 70 percent was strongly degraded. Southeast Asia followed with 24 percent experiencing human-induced degradation, 60 percent of which was severe. Twenty percent of Western Asia was degraded, 75 percent of which was strongly affected. Deserts were not included in these estimates.

Table 7. Extent of global human-induced land degradation[3]

	Extent of human-induced land degradation (Mha)		
Degradation	Global	Drylands	Humid
Total	1 660	733	927
Strong	850	418	432
Light	810	315	495

[3] Antarctica, Greenland, and land with more than 90 percent bare cover (the great deserts) were excluded. For humid areas, the cold zone where PET < 400 was excluded as well.

Table 8. Human-induced land degradation per SOLAW region[4]

Region	Area human-induced degradation (Mha)	Total area of region (Mha)	Affected (%)	Strongly degraded (Mha)	Slightly degraded (Mha)
Sub-Saharan Africa	330	2 413	14	149	181
Southern America	281	1 778	16	153	128
South Asia	180	439	41	126	54
Northern America	177	2 083	8	82	95
East Asia	156	1 185	13	84	72
Western Asia	123	615	20	92	31
Southeast Asia	122	501	24	74	48
Australia and New Zealand	94	796	12	34	59
Eastern Europe and Russian Federation	83	1 763	5	21	62
Western and Central Europe	56	489	11	12	44
Central Asia	31	456	7	12	19
Northern Africa	22	579	4	9	13
Central America and Caribbean	11	76	14	5	5
Pacific Islands	0.14	7	2	0.11	0.03
World	**1 660**	**13 178**	**13**	**850**	**810**
High-income	393	3 817	10	175	218
Upper middle-income	621	5 604	11	326	295
Lower middle-income	428	2 207	19	241	187
Low-income	220	1 520	14	107	112
Low-income and food-deficit	283	2 062	14	133	149
Least-developed	288	2 097	14	134	154

[4] Percentage of region extent refers to the portion of the total regional extent that is degraded. Antarctica, Greenland, and land with more than 90 percent bare cover (the great deserts) were excluded.

Figure 8. Frequency of variables responsible for the negative trend in regions affected by human-induced land degradation

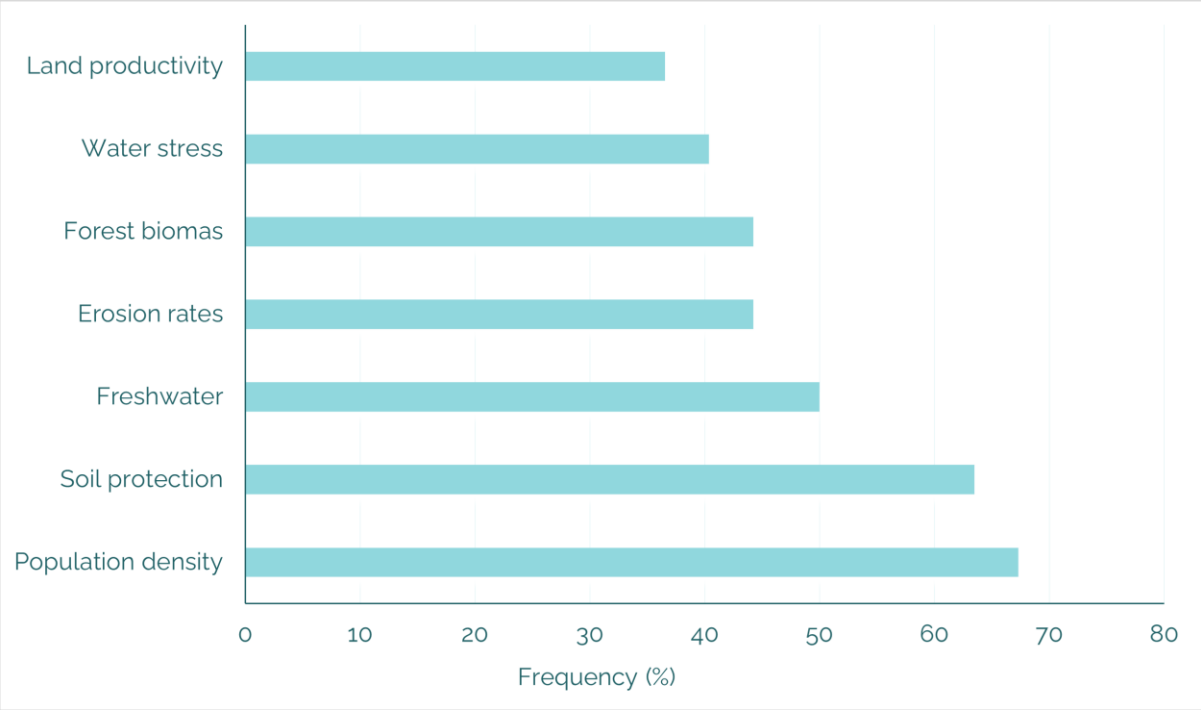

Source: Authors elaboration.

Increasing population density was the most common variable contributing to a negative trend in the 52 identified concentrations of human-induced land degradation, with an occurrence of 67 percent, followed by decreasing soil protection with 63 percent, and decreasing availability of freshwater with 50 percent (see Figure 8).

3.5. Discussion

A low status was found in drylands or mountains and seems to be related to climate and geomorphology. However, it could be the result of severe degradation in historic times that has reached a new equilibrium and appears to be under natural conditions. Unfortunately, there is no technique to identify such areas with the current available datasets (Fisher *et al.*, 2018).

High pressure does not necessarily lead to human-induced land degradation. The land degradation drivers analysis showed that 3 576 Mha of land is under high pressure from human activities, slightly less than half of which (1 660 Mha) is subject to human-induced land degradation (see Table 9). This implies that more than half of the areas under high pressure are stable. Comparing the land degradation map with the status layer revealed that 82 percent of these areas have high status, suggesting that favourable land conditions impede the triggering of degradation processes.

At the global level, the biophysical status of 5 670 Mha land is in decline, 1 660 Mha or 29 percent of which can be attributed to human-induced land degradation. The remaining 71 percent is classified as subject to deterioration, which may be caused by natural processes or have an anthropogenic origin. About half of the deteriorated areas have low status (see Table 10). Areas with low status are likely to be more sensitive to degradation processes than areas with high status, and moderate pressures may suffice to trigger

human-induced land degradation. A closer look at areas with low status subject to deterioration showed that 656 Mha are under moderate pressure, equal to 12 percent of the overall global decline. Most of these areas are probably affected by human-induced land degradation, which means that approximately 41 percent of global decline can be attributed to human-induced land degradation.

A second reason to take a critical look at the 71 percent of land that is facing deterioration is that various key drivers for human-induced land degradation, such as land use change, inappropriate agricultural management, and industrial pollution and development were not or only partly covered in this study, resulting in an underestimation of the cumulative pressure of anthropogenic activity.

Under- or overestimation of drivers and trends also occurs because the impact is not adjusted to the national and regional context. Due to limited available information, stratification (see Section 2.8) was only applied to grazing density. This will be further discussed in Section 4.2.

Land productivity contributes least to the negative trend in regions affected by human-induced land degradation, with an occurrence of 37 percent (see Figure 8). This variable is used by the UNCCD (2017) as an indicator for degradation in the Global Land Outlook. Soil erosion, another variable frequently used as an indicator for land degradation, appeared in 44 percent of the identified regions affected by human-induced land degradation.

The integration of the various dimensions is a new approach to distinguishing human-induced land degradation from a decline in status due to natural processes. However, human and naturally-driven processes may interact so that no clear distinction can be made between the impact of anthropogenic and natural drivers (Barger *et al.*, 2018; Olsson *et al.*, 2019). For example, in half of the identified concentrations of degraded land, a change in freshwater availability is contributing to the negative trend. In 62 percent of the cases, this contribution is small or else the driver of the change is unknown. According to Rodell *et al.* (2018), in 8 percent of the cases the change is caused by natural climate variability leading to drought, for example. In 19 percent of cases, a combination of natural and human drivers is responsible for the change in freshwater availability and the driver is exclusively of anthropogenic origin in only 12 percent of the regions.

Table 9. Comparison of the extent of threatened areas

Areas	Extent (Mha)
Affected by deterioration of status	5 670
At risk	3 866
Under high cumulative pressure	3 576
Affected by human-induced land degradation	1 660

Table 10. Degradation class combined with status

Degradation class	Percentage low status	Percentage high status
Strong deterioration under low pressure	49	51
Light deterioration under low pressure	50	50
Stable under high pressure	18	82

4. Spatial relation between land degradation and areas at risk, and land cover

4.1 Land degradation and land cover

A summary of the spatial relationship between land degradation and the global land cover (Fischer *et al.*, 2021) is presented in Table 11. Detailed information on the distribution of land degradation classes across land cover, per SOLAW region and country group, can be found in Annex V.

Cropland was the most affected by human-induced land degradation. Although it only covers 15 percent of the analysed area, 29 percent of all degraded areas is accounted for by cropland. Almost a third of rainfed cropland and nearly half of irrigated land is subject to human-induced land degradation processes. In North Africa, West Asia and South Asia, 60 percent or more of the irrigated areas were subject to human-induced land degradation. A mere 38 percent of global irrigated land is in stable condition, the lowest of the land cover types analysed. Large areas of degraded irrigated land were mostly found in the northern hemisphere with the exception of Southeast Asia (see Figure 9).

In West Asia, agricultural expansion, grazing and accessibility are the drivers of degradation, while in the densely populated areas of South Asia and East Asia, good accessibility and high grazing density exert significant pressures on irrigated fields. Grazing, accessibility and deforestation drive environmental change in irrigated cropland in Southeast Asia. Grazing, accessibility and agricultural expansion contribute most of the pressure on irrigation in the eastern United States of America. For information on other areas, please consult Annex III.

The decline in status in West Asia and East Asia is mostly caused by the decreasing availability of freshwater, increasing water stress, decreasing soil protection and increasing population. Similar degradation processes are occurring in South Asia, minus the decreasing soil protection. Major degradation processes in Southeast Asia are: increasing erosion rates, rapidly decreasing forest biomass and increasing population densities.

Table 11. Land degradation classes for global land cover

Land cover	Area (Mha)	Degraded (Mha)	Deteriorated (Mha)	Stable (Mha)	Degraded (%)	Deteriorated (%)	Stable (%)
Cropland	1 527	479	268	780	31	18	51
Rainfed	1 212	340	212	660	28	17	54
Irrigated	315	139	57	120	44	18	38
Grassland	1 910	246	642	1 022	13	34	54
Trees	4 335	485	1 462	2 388	11	34	55
Shrubs	1 438	218	584	636	15	41	44
Herbs	203	16	51	136	8	25	67
Sparse vegetation	1 034	85	499	450	8	48	44
Protected area	980	76	361	443	9	41	50

Figure 9. Large contiguous areas of irrigated cropland subject to human-induced land degradation

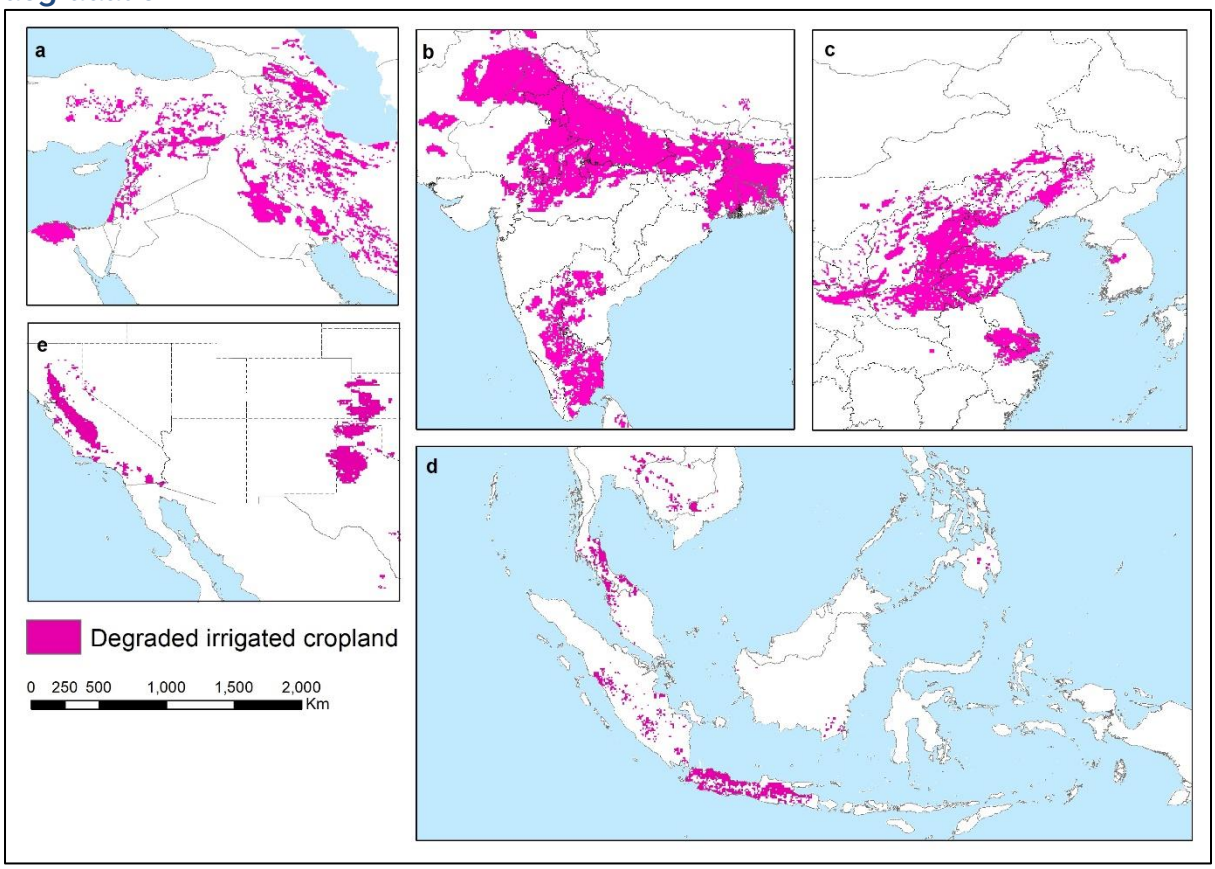

Source: United Nations Geospatial. 2020. Map geodata https://www.un.org/geospatial/file/3420. New York, USA, United Nations, modified by the author.

Notes: Dotted line represents approximately the Line of Control in Jammu and Kashmir agreed upon by India and Pakistan. The final status of Jammu and Kashmir has not yet been agreed upon by the parties.

a = North Africa and West Asia, b = South Asia, c = East Asia, d = Southeast Asia, e = North America. Areas with more than 10% irrigated cropland cover are shown.

In the eastern United States of America, a decline in available freshwater and loss of soil protection are the main contributors to degradation, with rising population density as an additional pressure in California. Annex IV presents the combinations of negative trends for all identified large contiguous areas of human-induced land degradation.

Although protected areas are largely free from land degradation, 41 percent are subject to deteriorating ecological conditions. A possible explanation for the high degree of deterioration in protected areas is that, despite diminished human pressure, degradation processes have continued because certain ecological thresholds were exceeded in the past. Another explanation could be that protected areas are often situated in remote areas that are difficult to access, with limited human activity. The first explanation is difficult to prove but the latter can be confirmed by analysing the degradation map: the most affected nature reserves are found in poorly accessible parts of Western Siberia and the Amazon Basin. Protected areas in West Siberia are affected by decreasing freshwater and those in the Amazon Basin suffer from loss of soil protection and forest biomass. Half of the protected areas are in stable or improving condition.

Table 12. Area agricultural land and forest at risk

Land cover	Total area (Mha)	Area at risk (Mha)	Percentage area at risk
Cropland	1527	472	31
Rainfed	1212	322	27
Irrigated	315	151	48
Grassland	1910	660	35
Forestland	4335	1112	26

Herbaceous vegetation is least affected by degradation and deterioration processes: 67 percent of the area occupied by such vegetation is stable or improving, followed by forest and grassland, with 55 percent and 54 percent in stable or improving condition respectively.

4.2 Agricultural land and forest at risk

The analysis of areas at risk is an alternative approach to studying decline in ecosystems services. Here, biophysical status is given as much importance as trend and no distinction is made between anthropogenic and natural causes. The concept may be useful for assessing the impact of decline. Areas with low biophysical status and strong decline are considered at risk. Areas with high biophysical status and slight decline are not considered at risk, nor are stable or improving areas.

The extent of cropland at risk (see Table 12) is similar to the extent of degraded croplands (see Table 11). The distribution of irrigated land at risk matches quite well with the distribution of degraded irrigated land. Although the global pattern of rainfed cropland at risk resembles that of degraded rain-fed land, closer inspection at the regional level reveals that both types occur side by side but that there is little overlap.

Cropland at risk (see Figure 10) includes lands that have been recently taken into use, are experiencing a decrease in freshwater and an increase in population density. Most grasslands at risk are face decreasing freshwater, with the exception of those situated in South America and sub-Saharan Africa where decreasing land productivity and soil protection account for the decline in ecosystem services. In Asia, increasing water stress also puts grasslands at risk. In sub-Saharan Africa, grasslands are prone to frequent and intense fires. Forestland at risk is prone to deforestation and, in sub-Saharan Africa, to frequent and intense fires as well. Forests at risk are affected by decreasing freshwater, loss of soil protection and forest biomass. The biophysical status of most regions at risk is characterized by low soil organic matter content and low plant species biodiversity.

Figure 10. Global distribution of agricultural land and forests at risk

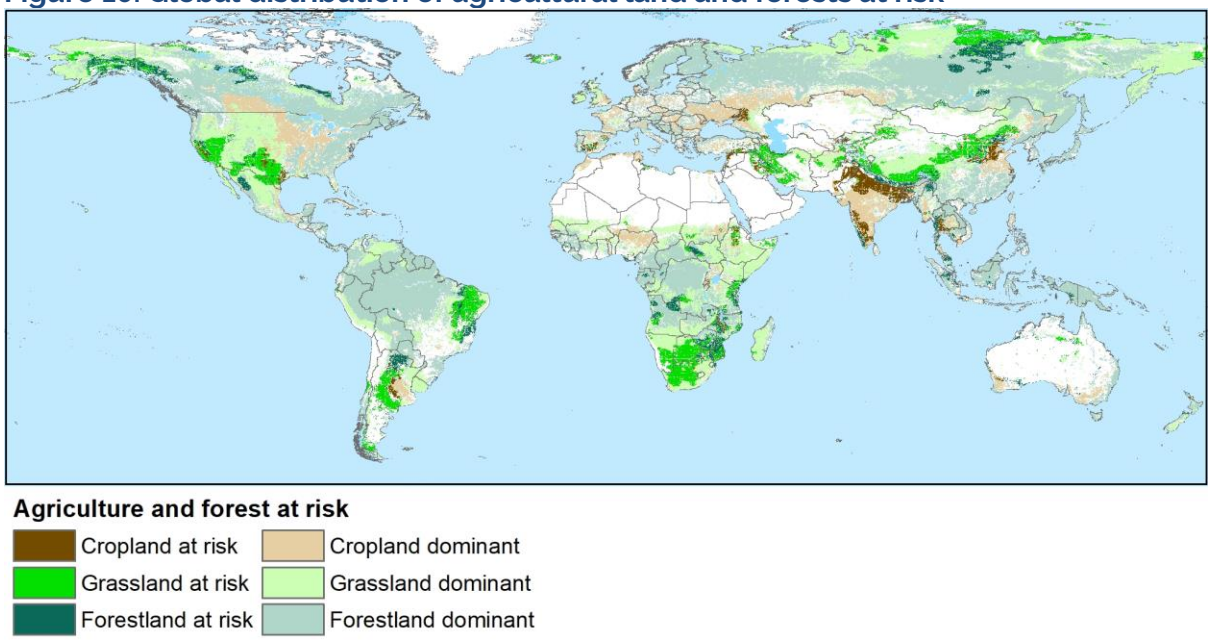

Source: United Nations Geospatial. 2020. Map geodata https://www.un.org/geospatial/file/3420. New York, USA, United Nations, modified by the author.

Notes: Final boundary between the Sudan and South Sudan has not yet been determined. Dotted line represents approximately the Line of Control in Jammu and Kashmir agreed upon by India and Pakistan. The final status of Jammu and Kashmir has not yet been agreed upon by the parties.

5. Evaluation of the multidimensional approach

5.1 Comparison of results with other land degradation studies

Gibbs and Salmon (2015) compared various global degradation assessments and found that estimates of degraded land range from 460 Mha to 6 140 Mha. The large discrepancy can be explained by the methodology applied (i.e., expert opinion versus GIS or modelling approach), the definition of land degradation that was used, and the quality of the input data.

A limited understanding of degradation processes, including the interaction of local geo-ecological conditions and socioeconomic drivers, complicates the assessment of land degradation on a global scale. Given the complexity and different perceptions of land degradation, it is not feasible to compile a land degradation map that will be received with universal approval and consequently, the World Atlas of Desertification (Cherlet *et al.,* 2018) decided to refrain attempting to produce such a map.

The methodology used for this global study was based on GLADIS (Nachtergaele *et al.*, 2011) and adopted the 'convergence of evidence' concept developed by Cherlet *et al.* (2018) for the World Atlas of Desertification (WAD). The concept of 'convergence of evidence' argues that areas with overlapping global change issues (GCIs) (e.g. water scarcity, deforestation, fire, population change and grazing density) may be subject to land degradation. The outputs of the three approaches showed similar results in regions most affected by land degradation, but differed in other areas.

The differences in output can be explained by the quantity, quality and categorization of the input layers. GLADIS and WAD had more spatial information at their disposal and applied stratification to most layers, though at the time GLADIS was developed images were not as accurate as currently. In terms of content, the role of the input layers is interpreted differently. This study regarded status as a description of current biophysical conditions, which included not only carbon stocks or biodiversity but also erosion processes. Trends were strictly limited to quantitative changes in a variable over time such as changes in erosion rate. GLADIS on the contrary, categorized processes as trends. This study only considered anthropogenic direct drivers, as defined by Barger *et al*. (2018), to assess pressure exerted by human activity, while the GCIs in WAD are a combination of trends and both natural and anthropogenic drivers.

A comparison with WAD is difficult because no map of land degradation was produced for that study. Nevertheless, in many regions, the evidence of convergence map produced for WAD showed similar patterns to the land degradation map produced for this report, i.e., the locations of areas with a high concentration of GCIs were reasonably consistent with areas exposed to human-induced land degradation.

In the Indo-Gangetic plains of India and Pakistan, southwest India and the North China plain, many GCIs coincide, suggesting the presence of human-induced land degradation. The concentration of GCIs in the lower Nile valley, the arc of degradation in northern West Asia and the most western part of Yemen suggest that these areas are subject to human-induced land degradation as well. The high concentration of GCIs in the eastern part of Central Asia was not recognized in this study. In Australia and New Zealand, the patterns do not coincide very well.

The southern Great Plains, the coastal zone of Texas and the southeastern United States of America are identified by WAD and this report as regions that are very likely exposed to human-induced land degradation. Both studies show similar patterns in the densely populated lowlands of northwest Europe, the Iberian Peninsula and the Po plain. In Ireland, Switzerland, Sicily, southeast Italy and the historical Macedonia region however, the patterns differ greatly.

In sub-Saharan Africa, there are some regions where a number of GCIs converge overlap with human-induced degraded areas as identified by this study; in other areas such as the Sahel, the reports differ. The WAD identifies a concentration of GCIs in the Sahel, whereas this study suggests that large areas are stable or improving, which confirms findings on the greening of the Sahel seen in recent studies (Fisher *et al*. 2018).

The pattern of convergence of GCIs in the northern part of South America resembles the distribution of human-induced degraded areas, such as the coastal plain of Ecuador and the Caribbean coast of Colombia, found in this study. The effect of the paved highway from Cuiabá (Mato Grosso) to Porto Velho (Rondônia) and Rio Branco (Acre) in the southwestern Brazilian Amazon is clearly visible in both studies, as is the agricultural expansion following deforestation around Santa Cruz de la Sierra in east Plurinational State of Bolivia. However, in Uruguay and the eastern part of Brazil the similarities between the studies disappear.

5.2 Recommendations

The current study focused on biophysical conditions and changes and their relationship to human-induced environmental pressure. Unfortunately, the socioeconomic impact of land degradation was not included. An impact analysis would add an extra dimension to the assessment and increase its inclusiveness. The economic provision capacity is also lacking because most approaches are singularly focused on the production and profit side. In general, such economic assessments do not favour the sustainable use of natural resources. Alternative methods to value land that consider the environmental costs should be developed.

The approach to calculating status, trend and cumulative pressure indices using input layers compiled at the global scale works well for overall status but lacks adequate detail for the trend and driver analyses. To obtain better estimates for the impact of drivers and trends, variables should be stratified in correspondence with land use, climate and geomorphology. For example, drylands are likely to be more susceptible to high population densities than are humid areas. Also, a small decrease in the soil erosion rate will have a different impact on a nearly flat agricultural field than on a steep forested slope.

Expert consultations can reduce subjectivity in the normalization and classification procedures, which subsequently should be converted to standardized protocols to improve the transparency of the approach. Expert consultations could also contribute to the stratification process and verification of the results.

As mentioned in Sections 2.7 and 3.4.3, the use of readily available state-of-the-art maps constrained the selection of input layers. For example, the calculation of the overall status index would benefit if information on animal biodiversity and pollution by agriculture, mining and industry could be added to the analysis. The overall trend index would benefit

from data on changes in soil properties, biodiversity and pollution. Land use change as the main driver for degradation could be represented by gain and loss of forest, crop and grazing land cover. Nutrient deficit and surplus could serve as an indicator for agricultural management, and industrial development could be represented by data on infrastructure, mining and built-up areas.

6. Conclusions

There is a strong correlation between water-related issues and human-induced land degradation. Increasing SFV water stress and decreasing freshwater availability are prominent in large contiguous degraded areas worldwide. Such an overlap was not found for land productivity – which is used by the UNCCD – or soil erosion – another generally accepted indicator for land degradation.

Of the main land cover types, cropland is the most affected by human-induced land degradation. The extent to which irrigated land in particular has been degraded indicates widespread, unsustainable agricultural practices under high pressures.

In relative terms, the most affected region is South Asia, where nearly half of the land is subject to man-made degradation, most of it severe. Southeast Asia and Western Asia are also strongly affected.

Grazing is the most common occurring driver of human-induced degradation, followed by accessibility and agricultural expansion.

A significant part of the areas characterized by a negative overall trend were not exposed to recent high pressure by human activities onsite. Neither are areas under high pressure necessarily subject to land degradation. The response to pressure can be partly attributed to resilience, as evidenced by status: areas under high pressure with favourable biophysical conditions are less prone to land degradation. Areas with a low status are more sensitive and a moderate pressure might suffice to trigger degradation. Also, degradation processes that started in the past can continue when certain thresholds are exceeded, even if the pressure of human activities has decreased or ceased. Another possible explanation is that human-induced climate change has altered local temperature and precipitation regimes, thereby exacerbating natural processes.

This study builds on the pioneering work of Nachtergaele *et al.* (2011) who developed the Global Land Degradation Information System (GLADIS) at a time when high-quality geospatial data were not as abundant as they are today. The cumulative effect of direct anthropogenic drivers, which represent the human pressure on a system, is an additional dimension to the already existing dimensions of status and trend. The integration of three dimensions of land degradation provide us with insights into the spatial relationships between land conditions, degradation processes and the pressure of human activity. The land degradation analysis verifies whether a decline in ecosystem services is of anthropogenic origin and hence can be classified as human-induced land degradation. The areas at risk analysis does not discriminate between human and natural causes but estimates the potential impact of deteriorating ecosystem services.

Fine tuning of the methodology, e.g. by adjusting the impact of trend and drivers at the regional and national levels, is required to identify more accurately which part of the decline in soil, water and vegetation properties can be classified as land degradation. However, because natural and human-induced processes may interact, it is not always possible or relevant to make a distinction.

7. References

Archibald, S., Lehmann, C.E.R., Gómez-Dans, J.L. & Bradstock, R.A. 2013. Defining pyromes and global syndromes of fire regimes. *Proceedings of the National Academy of Sciences of the United States of America*, 110(16): 6442–6447. (also available at https://doi.org/10.1073/pnas.1211466110).

Barger, N.N., Gardner, T.A., Sankaran, M., Belnap, J., Broadhurst, L., Brochier, V., Isbell, F. *et al.* 2018. Direct and indirect drivers of land degradation and restoration. *In* L. Montanarella, R. Scholes & A. Brainich, eds. *The IPBES assessment report on land degradation and restoration*, pp. 137–218. Bonn, Germany, Intergovernmental Science-Policy Platform on Biodiversity and Ecosystem Services (IPBES).

Borrelli, P., Robinson, D.A., Fleischer, L.R., Lugato, E., Ballabio, C., Alewell, C., Meusburger, K. *et al.* 2017. An assessment of the global impact of 21st century land use change on soil erosion. *Nature Communications*, 8(1). (also available at https://doi.org/10.1038/s41467-017-02142-7).

Carrillo, Y., Guarín, A. & Guillot, G. 2006. Biomass distribution, growth and decay of Egeria densa in a tropical high-mountain reservoir (NEUSA, Colombia). *Aquatic Botany*, 85(1): 7–15. (also available at https://doi.org/10.1016/j.aquabot.2006.01.006).

Center for International Earth Science Information Network (CIESIN). 2018. *Gridded Population of the World, Version 4 (GPWv4): population density, Revision 11* [online]. [Cited 1 March 2020]. https://sedac.ciesin.columbia.edu/data/set/gpw-v4-population-density-rev11/data-download

Cherlet, M., Hutchinson, C., Reynolds, J., Hill, J., Sommer, S. & von Maltitz, G., eds. 2018. *World Atlas of Desertification*. Luxembourg, Publication Office of the European Union. 248 pp.

Conti, G., Gorné, L.D., Zeballos, S.R., Lipoma, M.L., Gatica, G., Kowaljow, E., Whitworth-Hulse, J.I. *et al.* 2019. Developing allometric models to predict the individual aboveground biomass of shrubs worldwide. *Global Ecology and Biogeography*, 28(7): 961–975. (also available at https://doi.org/10.1111/geb.12907).

Ellis, E.C., Antill, E.C. & Kreft, H. 2012. All is not loss: plant biodiversity in the anthropocene. *PLoS ONE*, 7(1): e30535 [online]. [Cited 9 September 2021]. https://doi.org/10.1371/journal.pone.0030535

Estrada, G. & Soares, M.L.G. 2017. Global patterns of aboveground carbon stock and sequestration in mangroves. *Anais da Academia Brasileira de Ciências*, 89(2): 973–989. (also available at https://doi.org/10.1590/0001-3765201720160357).

European Union. 2003. Global Land Cover 2000 database. In: *Joint Research Centre (JRC)* [online]. [Cited 1 March 2020]. https://forobs.jrc.ec.europa.eu/products/glc2000/glc2000.php

Fischer, G., Nachtergaele, F.O., van Velthuizen, H.T., Chiozza, F., Franceschini, G., Henry, M., Muchoney, D. & Tramberend, S. 2021. *Global agro ecological zones v4 – model documentation*. Rome, Food and Agriculture Organization of the United Nations (FAO). 306 pp.

Fisher, J., Montanarella, L. & Scholes, R. 2018. Benefits to people from avoiding land degradation and restoring degraded land. *In* L. Montanarella, R. Scholes & A. Brainich, eds. *The IPBES assessment report on land degradation and restoration*, pp. 1–51. Bonn, Secretariat of the Intergovernmental Science-Policy Platform on Biodiversity and Ecosystem Services.

Food and Agricultural Organization of the United Nations (FAO). 2013. *Mapping land use systems at global and regional scales for land degradation assessment analysis Version 1.1*. Rome, FAO. 20 pp.

FAO & Intergovernmental Technical Panel on Soils (ITPS). 2018. *Global Soil Organic Carbon Map (GSOCmap)*. Technical report. Rome, FAO. 162 pp. (also available at https://storage.googleapis.com/fao-maps-catalog-data/geonetwork/gsoc/GSOCmap/GSOCmap1.5.0.tif)

Gerten, D., Heck, V., Jägermeyr, J., Bodirsky, B.L., Fetzer, I., Jalava, M., Kummu, M. *et al.* 2020. Feeding ten billion people is possible within four terrestrial planetary boundaries. *Nature Sustainability*, 3(3): 200–208. (also available at https://doi.org/10.1038/s41893-019-0465-1).

Gibbs, H.K. & Salmon, J.M. 2015. Mapping the world's degraded lands. *Applied Geography*, 57: 12–21. (also available at https://doi.org/10.1016/j.apgeog.2014.11.024).

Gilbert, M., Nicolas, G., Cinardi, G., Van Boeckel, T.P., Vanwambeke, S.O., Wint, G.R.W. & Robinson, T.P. 2018. Global distribution data for cattle, buffaloes, horses, sheep, goats, pigs, chickens and ducks in 2010. In: *Scientific Data* [online]. [Cited 1 March 2020]. https://doi.org/10.1038/sdata.2018.227

Ginoux, P., Prospero, J.M., Gill, T.E., Hsu, N.C. & Zhao, M. 2012. Global-scale attribution of anthropogenic and natural dust sources and their emission rates based on MODIS Deep Blue aerosol products. *Reviews of Geophysics*, 50(3): 1–36. (also available at https://doi.org/10.1029/2012RG000388).

Global Runoff Data Centre (GRDC). 2020. *Major river basins of the world. 2nd edition* [online]. [Cited 1 March 2020]. https://www.bafg.de/GRDC/EN/Home/homepage_node.html

Guerra, C.A., Rosa, I.M.D., Valentini, E., Wolf, F., Filipponi, F., Karger, D.N., Nguyen Xuan, A., Mathieu, J., Lavelle, P. & Eisenhauer, N. 2020. Global vulnerability of soil ecosystems to erosion. *Landscape Ecology*, 35(4): 823–842. (also available at https://doi.org/10.1007/s10980-020-00984-z).

Hamdan, M.A., Asada, T., Hassan, F.M., Warner, B.G., Douabul, A., Al-Hilli, M.R.A. & Alwan, A.A. 2010. Vegetation response to re-flooding in the Mesopotamian wetlands, southern Iraq. *Wetlands*, 30(2): 177–188. (also available at https://doi.org/10.1007/s13157-010-0035-9).

Han, M., Pan, B., Liu, Y. Bin, Yu, H.Z. & Liu, Y.R. 2019. Wetland biomass inversion and space differentiation: A case study of the Yellow River Delta Nature Reserve. *PLoS ONE*, 14(2): e0210774 [online]. [Cited 9 September 2021]. https://doi.org/10.1371/journal.pone.0210774

Hansen, M.C.C., Potapov, P. V, Moore, R., Hancher, M., Turubanova, S.A. a, Tyukavina, A., Thau, D. *et al.* 2013. High-Resolution Global Maps of. *Science*, 342(November): 850–854. https://doi.org/10.1126/science.1244693

Intergovernmental Panel on Climate Change (IPCC). 2003. *Good Practice Guidance for Land Use, Land-Use Change and Forestry*. J. Penman, M. Gytarsky, T. Hiraishi, T. Krug, D. Kruger, R. Pipatti, L. Buendia, K. Miwa, T. Ngara, K. Tanabe & F. Wagner, eds. Hayama, Japan, IPCC. 590 pp.

Junk, W.J. & Piedade, M.T.F. 1993. Drought and aquatic community resilience: the role of eggs and seeds in sediments of temporary wetlands. *Hydrobiologia*, 263: 155–162.

Kreft, H. & Jetz, W. 2007. Global patterns and determinants of vascular plant diversity. *Proceedings of the National Academy of Sciences of the United States of America*, 104(14): 5925–5930. (also available at https://doi.org/10.1073/pnas.0608361104).

Latham, J., Cumani, R., Rosati, I. & Bloise, M. 2014. FAO Global Land Cover SHARE. In: *Database Beta-Release Version 1.0* [online]. [Cited 1 March 2020]. http://www.glcn.org/downs/prj/glcshare/GLC_SHARE_beta_v1.0_2014.pdf

Lonsdale; W.M. 1999. Global patterns of plant invasions and the concept of invasibility. *Ecology*, 80: 1522–1536.

Lou, Y., Pan, Y., Gao, C., Jiang, M., Lu, X. & Xu, Y.J. 2016. Response of plant height, species richness and aboveground biomass to flooding gradient along vegetation zones in floodplain wetlands, Northeast China. *PLoS ONE*, 11(4): e0153972 [online]. [Cited 9 September 2021]. https://doi.org/10.1371/journal.pone.0153972

Lumbierres, M., Méndez, P.F., Bustamante, J., Soriguer, R. & Santamaría, L. 2017. Modeling biomass production in seasonal wetlands using MODIS NDVI land surface phenology. *Remote Sensing*, 9(4): 1–18. (also available at https://doi.org/10.3390/rs9040392).

Miller, G.J., Morris, J.T. & Wang, C. 2019. Estimating aboveground biomass and its spatial distribution in coastal wetlands utilizing planet multispectral imagery. *Remote Sensing*, 11(17). (also available at https://doi.org/10.3390/rs11172020).

Montanarella, L., Scholes, R. & Brainich, A. eds. 2018. *The IPBES assessment report on land degradation and restoration*.. Bonn, Germany, Intergovernmental Science-Policy Platform on Biodiversity and Ecosystem Services. 744 pp.

Nachtergaele, F., Petri, M., Biancalani, R., van Lynden, G., van Velthuizen, H. & Bloise, M. 2011. *Global Land Degradation Information System (GLADIS) - an information database for land degradation assessment at global level. LADA Technical report n. 17*. Rome, FAO. 110 pp.

Olsson, L., Barbosa, H., Bhadwal, S., Cowie, A., Delusca, K., Flores-Renteria, D., Hermans, K. *et al.* 2019. Land degradation. *In* P.R. Shukla, J. Skea, E.C. Buendia, V. Masson-Delmotte, H.O. Pörtner, D.C. Roberts, P. Zhai *et al*., eds. *Climate change and land: an IPCC special report on climate change, desertification, land degradation, sustainable land management, food security, and greenhouse gas fluxes in terrestrial ecosystems*, pp. 345–436. Geneva, Switzerland, IPCC.

Peregon, A., Maksyutov, S., Kosykh, N.P. & Mironycheva-Tokareva, N.P. 2008. Map-based inventory of wetland biomass and net primary production in western Siberia. *Journal of Geophysical Research: Biogeosciences*, 113(1): 1–12. (also available at https://doi.org/10.1029/2007JG000441).

Qin, Y., Mueller, N.D., Siebert, S., Jackson, R.B., AghaKouchak, A., Zimmerman, J.B., Tong, D., Hong, C. & Davis, S.J. 2019. Flexibility and intensity of global water use. *Nature Sustainability*, 2(6): 515–523. (also available at https://doi.org/10.1038/s41893-019-0294-2).

Richts, A., Struckmeier, W.F. & Zaepke, M. 2011. Sustaining groundwater resources. *Sustaining Groundwater Resources*: 159–173. (also available at https://doi.org/10.1007/978-90-481-3426-7).

Robinson, T.P., William Wint, G.R., Conchedda, G., Van Boeckel, T.P., Ercoli, V., Palamara, E., Cinardi, G., D'Aietti, L., Hay, S.I. & Gilbert, M. 2014. Mapping the global distribution of livestock. *PLoS ONE*, 9(5): e96084 [online]. [Cited 9 September 2021]. https://doi.org/10.1371/journal.pone.0096084

Rodell, M., Famiglietti, J.S., Wiese, D.N., Reager, J.T., Beaudoing, H.K., Landerer, F.W. & Lo, M.H. 2018. Emerging trends in global freshwater availability. *Nature*, 557(7707): 651–659. (also available at https://doi.org/10.1038/s41586-018-0123-1).

Ruesch, A. & Gibbs, H.K. 2008. New IPCC Tier-1 Global Biomass Carbon Map for the year 2000. In: *Carbon Dioxide Information Analysis Center* [online]. [Cited 1 March 2020]. http://cdiac.ess-dive.lbl.gov

Santoro, M., Cartus, O., Carvalhais, N., Rozendaal, D., Avitabilie, V., Araza, A., de Bruin, S. *et al.* 2020. The global forest above-ground biomass pool for 2010 estimated from high-resolution satellite observations. In: *Earth System Science Data Discussions* [online]. [Cited 1 March 2020]. https://doi.pangaea.de/10.1594/PANGAEA.894711

Shukla, P.R., Skea, J., Buendia, E.C., Masson-Delmotte, V., Pörtner, H.O., Roberts, D.C., Zhai, P. *et al.*, eds. 2019. *Climate change and land: an IPCC special report on climate change, desertification, land degradation, sustainable land management, food security, and greenhouse gas fluxes in terrestrial ecosystems*. Geneva, Switzerland, Intergovernmental Panel on Climate Change (IPCC).

Truus, L. 2011. Estimation of above-ground biomass of wetlands. *Biomass and remote sensing of biomass*: [online]. [Cited 9 September 2021]. http://dx.doi.org/10.5772/18390.

United Nations Convention to Combat Desertification (UNCCD). 2017. *The global land outlook*. First edition. Bonn, Germany, United Nations Convention to Combat Desertification. 340 pp.

Weiss, D.J., Nelson, A., Gibson, H.S., Temperley, W., Peedell, S., Lieber, A., Hancher, M. *et al.* 2018. A global map of travel time to cities to assess inequalities in accessibility in 2015. *Nature*, 553(7688): 333–336. (also available at https://doi.org/10.1038/nature25181).

Annex I. Resolution of input layer and location of dataset

ID	Input layer	Resolution of source layer	Available at
1	Soil nutrient availability	5 arc minutes	GAEZ v4
2	Soil organic carbon	30 arc seconds	http://54.229.242.119/GSOCmap/
3	Soil water erosion rate	30 arc seconds	https://figshare.com/s/d7918be095b8794f8eed
4	Wind erosion	6 arc minutes	https://agupubs.onlinelibrary.wiley.com/doi/10.1029/2012RG000388
5	Groundwater recharge	ca 120 arc minutes	https://www.whymap.org
6	SFV water stress	5 arc minutes	https://doi.org/10.1038/s41893-019-0294-2
7	Native species	480 arc minutes	http://ecotope.org/products/datasets/
8	Above ground biomass	5 arc minutes	http://globbiomass.org/products/global-mapping
9	Urbanization	30 arc seconds	http://www.fao.org/geonetwork/srv/en/main.home?uuid=ba4526fd-cdbf-4028-a1bd-5a559c4bff38
10	Soil erosion change	12.5 arc minutes	https://esdac.jrc.ec.europa.eu/themes/global-soil-erosion
11	Soil protection change	30 arc seconds	https://figshare.com/s/d7918be095b8794f8eed
12	Changes in available fresh water	180 arc minutes	https://search.earthdata.nasa.gov/
13	SFV water stress change	5 arc minutes	https://doi.org/10.1038/s41893-019-0294-2
14	Land productivity	30 arc seconds	https://wad.jrc.ec.europa.eu/geoportal
15	Above ground forests biomass change	5 arc minutes	http://cdiac.ess-dive.lbl.gov
16	Population density change	5 arc minutes	https://sedac.ciesin.columbia.edu/data/set/gpw-v4-population-density-rev11
17	Agricultural expansion	30 arc seconds	http://www.fao.org/geonetwork/srv/en/main.home?uuid=ba4526fd-cdbf-4028-a1bd-5a559c4bff38

ID	Input layer	Resolution of source layer	Available at
18	Deforestation	1 arc second	earthenginepartners.appspot.com/science-2013-global-forest
19	Fire combined	30 arc minutes	Data provided by S. Archibald
20	Grazing density	5 arc minutes	http://www.fao.org/livestock-systems/global-distributions/en/
21	Accessibility	30 arc seconds	https://malariaatlas.org/research-project/accessibility_to_cities/
22	Invasive/native ratio	480 arc minutes	http://ecotope.org/products/datasets/

Annex II: Contributing factors to a deterioration of status per region

Pop dens = population density; Water stress = SFV water stress; Land product = land productivity

Region	Freshwater availability	Pop dens	Soil protection	Water stress	Forest biomass	Erosion rates	Land product
Southern Alaska to south-west Yukon	X						
Hudson Bay area	X						
British Columbia	X		X				X
Northern Alberta & Saskatchewan, Northwest Territories	X						X
Western Washington		X			X		
California	X	X	X				
Nevada	X						
Texas	X	X	X	X	X		X
Southeast United States of America		X	X		X		
Sierra Madre Occidental, Mexico	X		X		X		
Yucatan & Caribbean coast, Central America		X	X		X	X	
Iceland	X						
Spain		X		X			
East Ukraine to west Kazakhstan	X		X				X
Siberia	X						X
Syrian Arab Republic, Lebanon, Israel and Jordan	X	X					
Northern West Asia	X			X			
Western Yemen	X	X					
East Pakistan to Bangladesh	X	X		X			
South India	X	X		X	X		
Hindu Kush, Pamirs &Tien Shan	X			X			
Karakoram & eastern Kunlun Shan	X	X		X			
South & east Tibet	X	X	X	X			

Pop dens = population density; Water stress = SFV water stress; Land product = land productivity

Region	**Freshwater availability**	**Pop dens**	**Soil protection**	**Water stress**	**Forest biomass**	**Erosion rates**	**Land product**
Loess Plateau to Bohai Sea, China	X	X	X	X			
Coastal zone, southeast China		X			X	X	
Irrawaddy valley, Myanmar	X			X		X	
South Cambodia	X	X	X	X			
Vietnam		X	X		X	X	
West Thailand	X			X			
Malay peninsula	X		X	X	X		X
Filipinas	X	X	X		X	X	
Borneo	X	X	X		X	X	
Papua	X	X	X		X		
West Australia			X	X			X
Southeast Australia	X		X				X
Northern Nile valley	X	X		X			
Ethiopian Highlands			X	X		X	
East & southeast Africa	X	X			X		
Southern Africa			X	X			X
Congo basin	X	X			X		
West Africa		X	X		X		
Amazon			X		X		
East Brazil	X		X	X		X	
Santa Cruz, Plurinational State of Bolivia			X	X	X		X
Chaco, north Argentina & western Paraguay			X	X	X		X
Central & south Argentina	X	X	X			X	
Total occurrence	**33**	**26**	**26**	**18**	**17**	**11**	**10**
Percentage of total	**72**	**57**	**57**	**39**	**37**	**24**	**22**

Annex III: Main drivers per region subject to high human induced pressure

Pop dens = population density; Deforest = deforestation; Invasive spp = invasive species

Region	Grazing	Pop dens	Agricultural expansion	Deforest	Invasive spp	Fire
Southern Alberta & Saskatchewan	X		X			
British Columbia				X	X	
Southwest Nebraska to Northwest Texas	X		X			
West Coast United States of America		X		X	X	
East Coast United States of America		X		X	X	
Florida	X	X	X	X	X	
Texas	X	X	X			
Mexico	X	X	X			
Greater Antilles	X	X				
Pacific coast, Central America	X	X	X			
North Europe	X			X		
West and East Europe	X	X	X		X	
Volga basin, Russian Federation		X	X		X	
Northern Kazakhstan			X			X
Northern West Asia	X	X	X			
Western Yemen	X	X				
East Pakistan	X	X				
India	X	X	X			
Bangladesh	X	X				
Central east China	X	X			X	
South east China	X	X		X		
Korea's		X			X	
Japan		X			X	
Irrawaddy valley, Myanmar	X	X	X			
East Thailand	X	X	X			
South Cambodia	X	X	X	X		
Vietnam	X	X	X	X		
Filipinas	X	X	X			
Java	X	X	X			

Pop dens = population density; Deforest = deforestation; Invasive spp = invasive species

Region	Grazing	Pop dens	Agricultural expansion	Deforest	Invasive spp	Fire
North Australia						X
Southwest Australia	X		X			X
Southeast Australia	X		X	X	X	
North Island, New Zealand	X			X	X	
Maghreb	X	X	X			
Northern Nile Valley	X	X				
Ethiopian highlands	X	X	X			
South Sudan	X					X
Uganda		X	X			X
Lake Victoria region	X	X	X			
Nigeria	X	X	X			
West African coast		X	X	X		
Southeast and southwest Congo basin						X
Northeast border region of Namibia			X			X
Southeast Africa	X	X	X	X		
Eastern and southern Atlantic coast, Brazil	X	X	X			
Along border of Plurinational State of Bolivia, Paraguay and Argentina with Brazil			X	X		
Eastern Parana and Tocantins basin, Brazil	X			X		X
Uruguay	X					
Buenos Aires province, Argentina	X		X			
South central Chile	X	X	X	X	X	
Santa Cruz, Plurinational State of Bolivia		X	X	X		
Peru	X	X	X			
Coastal plain, Ecuador	X	X	X			X
Inter-Andean valley, Ecuador	X	X				
Cauca and Magdalena valles, Colombia	X	X	X			
Western Bolivarian Republic of Venezuela	X	X	X			
Total occurrence	**42**	**40**	**36**	**16**	**12**	**9**
Percentage of total	**75**	**71**	**64**	**29**	**21**	**16**

Annex IV: Degradation processes per contiguous degraded area

Water stress = SFV water stress; Pop dens = population density; Land product = land productivity

Large degraded areas	Freshwater availability	Water stress	Pop dens	Soil protection	Erosion rates	Forest biomass	Land product
British Columbia	X			X			X
Western Washington			X			X	
California	X		X	X			
Central Idaho				X	X	X	X
Southwest Nebraska to northwest Texas				X			X
Southeast Texas	X	X	X	X			X
Southeast United States of America			X	X		X	
Yucatan peninsula	X		X	X		X	
Switzerland	X		X				
Pais Vasco		X	X	X		X	
Galicia			X	X	X	X	
West Andalusia		X	X		X	X	X
Central Ukraine to southwest Russian Federation	X			X			X
Russian Federation, near northwestern Kazakhstan	X						
Northwest Kazakhstan	X			X			X
Central Anatolia		X	X				
West Asia	X	X	X	X			X
Western Yemen	X		X				
East Uzbekistan	X		X	X			
East Pakistan to Bangladesh	X	X	X				
South India	X	X	X			X	
Loess Plateau to Bohai Sea, China	X	X	X	X			
Central Irrawaddy valley, Myanmar		X		X	X		
Cambodia	X	X	X	X	X		X
Malay peninsula	X		X		X	X	
Sumatra			X	X	X	X	
Java			X		X	X	

Water stress = SFV water stress; Pop dens = population density; Land product = land productivity

Large degraded areas	Freshwater availability	Water stress	Pop dens	Soil protection	Erosion rates	Forest biomass	Land product
Northwest Australia	X			X			X
Northeast Australia						X	X
Central Maghreb	X	X	X	X	X		X
Nile delta		X	X				
Ethiopian Highlands		X		X	X		
Eastern Central African Republic - Western South Sudan	X	X				X	
Uganda		X	X	X	X	X	
Southern Kenya - Northern Tanzania		X	X	X	X		
Coastal Tanzania			X	X	X	X	X
Northeastern Zambia	X		X		X	X	
Southern Malawi - Northern Mozambique			X		X	X	
Mozambique - Zimbabwe - Eswatini border region	X	X	X	X		X	
Botswana				X			X
Southwestern Madagascar			X	X	X	X	
Southern Angola			X	X		X	X
Northeastern Angola - Southwestern Congo	X			X	X	X	
West Africa			X		X	X	
Eastern and southern Atlantic coast, Brazil	X		X		X		
Western Sao Francisco basin, Brazil	X	X					
Uruguay	X			X	X		
Buenos Aires province, Argentina				X	X		X
Chaco, north Argentina & western Paraguay		X		X		X	X
Santa Cruz, Plurinational State of Bolivia			X	X	X		X
South central Chile	X	X	X	X	X		
Coastal plain, Ecuador		X	X				X

Annex V: Land degradation classes per SOLAW regions and country groups

Deg = degradation; det = deterioration

	Total area (Mha)	Strong deg (Mha)	Light deg (Mha)	Strong det (Mha)	Light det (Mha)	Stable-high pressure (Mha)	Stable-low pressure (Mha)	Deg (%)	Det (%)	Stable (%)
Australia & New Zealand										
Rainfed agriculture	44	4	6	4	6	10	15	21	21	58
Irrigation	3	0.21	0.38	0.21	0.41	0.91	1.1	18	19	63
Grassland	69	2.3	4	11	17	6	29	9	40	51
Shrubs	19	0.53	0.67	4	6	0.79	7	6	56	38
Trees	131	11	18	19	24	25	34	22	33	45
Herbs	0.33	0.016	0.045	0.054	0.067	0.058	0.093	18	36	45
Sparse vegetation	513	16	30	108	153	39	167	9	51	40
Sum land cover	781	34	59	146	207	82	253	12	45	43
Protected area	61	3	4	11	15	8	20	12	42	46
Central Asia										
Rainfed agriculture	28	0.69	1.5	1.2	5	5	14	8	24	68
Irrigation	13	1.1	1.7	0.7	1.3	4	4	22	16	62
Grassland	73	1.5	3	8	14	10	35	6	31	63
Shrubs	20	0.52	1.1	1.3	3	4	10	8	22	69
Trees	26	0.6	1.3	2	4	5	14	7	21	72
Herbs	1.3	0.03	0.03	0.47	0.27	0.1	0.42	4	56	40
Sparse vegetation	96	7	8	12	19	15	35	16	32	53
Sum land cover	256	11	17	25	47	44	112	11	28	61
Protected area	7	0.1	0.52	1.3	1.3	0.78	3	9	38	52
Central America & Caribbean										
Rainfed agriculture	13	1.1	1.3	1.1	0.8	6	2.3	18	15	67
Irrigation	2	0.12	0.18	0.1	0.1	1.1	0.39	15	10	75
Grassland	11	0.74	0.92	1.5	1.1	4	3	15	23	63
Shrubs	4	0.32	0.36	0.73	0.39	1.4	0.92	16	27	56
Trees	38	3	2.3	11	6	8	9	13	43	44
Herbs	0.3	0.0009	0.007	0.05	0.04	0.07	0.2	2	27	71
Sparse vegetation	0.03	0.0004	0.001	0.008	0.002	0.003	0.015	4	36	61
Sum land cover	68	5	5	14	8	21	16	14	32	53
Protected area	10	0.17	0.16	3	2.3	0.71	3	3	58	38

Deg = degradation; det = deterioration

	Total area (Mha)	Strong deg (Mha)	Light deg (Mha)	Strong det (Mha)	Light det (Mha)	Stable-high pressure (Mha)	Stable-low pressure (Mha)	Deg (%)	Det (%)	Stable (%)
East Asia										
Rainfed agriculture	60	10	9	1.9	3	26	11	31	7	61
Irrigation	73	19	10	4	4	26	10	41	11	49
Grassland	347	20	15	70	74	30	138	10	42	49
Shrubs	57	4	4	6	7	16	20	15	22	63
Trees	275	16	25	18	28	97	91	15	17	68
Herbs	0.1	0.03	0.01	0.02	0.01	0.01	0.03	31	25	44
Sparse vegetation	69	0.95	0.84	9	18	3	37	3	39	58
Sum land cover	881	71	64	109	133	197	307	15	27	57
Protected area	19	0.57	0.65	4	4	2	8	7	41	53
East Europe & Russian Federation										
Rainfed agriculture	160	10	25	13	26	57	29	22	24	54
Irrigation	6	0.6	0.9	0.8	1.2	1.6	1.2	24	32	44
Grassland	314	4	13	19	78	35	163	6	31	63
Shrubs	99	0.36	1.1	4	22	5	66	1	27	72
Trees	915	3	17	17	163	118	597	2	20	78
Herbs	73	0.2	0.8	1.6	14	4	52	1	22	77
Sparse vegetation	5	0.1	0.14	0.35	1.1	0.35	3	5	29	66
Sum land cover	1571	19	59	55	306	221	912	5	23	72
Protected area	146	1	3	8	33	16	85	3	28	69
North Africa										
Rainfed agriculture	21	3	5	0.4	0.7	11	1.5	35	5	59
Irrigation	6	2	1.6	0.24	0.2	1.5	0.43	60	7	33
Grassland	6	0.55	0.78	0.56	0.48	2.4	0.78	24	19	58
Shrubs	5	0.49	0.6	0.2	1.28	1.8	0.66	22	29	49
Trees	6	0.34	0.82	0.3	1.33	2.2	0.93	20	28	53
Herbs	0.8	0.05	0.05	0.02	0.34	0.03	0.28	13	46	40
Sparse vegetation	22	0.9	2.2	1.1	5	6	7	14	27	59
Sum land cover	66	7	11	3	9	25	11	27	18	55
Protected area	1.1	0.06	0.03	0.02	0.53	0.05	0.45	8	48	44

Deg = degradation; det = deterioration

	Total area (Mha)	Strong deg (Mha)	Light deg (Mha)	Strong det (Mha)	Light det (Mha)	Stable-high pressure (Mha)	Stable-low pressure (Mha)	Deg (%)	Det (%)	Stable (%)
North America										
Rainfed agriculture	198	13	15	3	4	94	68	14	4	82
Irrigation	34	5	4	2.2	2.1	12	7	29	13	58
Grassland	260	13	13	31	39	50	115	10	27	63
Shrubs	368	11	9	61	93	24	169	5	42	53
Trees	692	27	41	58	93	193	280	10	22	68
Herbs	73	4	5	3	11	13	38	12	19	69
Sparse vegetation	174	1.2	1.3	52	38	3	78	1	52	47
Sum land cover	1799	74	89	210	281	390	755	9	27	64
Protected area	159	4	3	34	35	10	73	5	43	52
Pacific islands										
Rainfed agriculture	0.46	0.02	0.01	0.12	0.07	0.03	0.21	6	42	52
Irrigation	0.004	0.0003	0	0.001	0.0002	0.001	0.002	8	30	62
Grassland	0.49	0.01	0.002	0.17	0.06	0.012	0.23	2	47	51
Shrubs	0.3	0.008	0.002	0.12	0.04	0.009	0.12	3	53	44
Trees	3.74	0.056	0.02	1.6	0.46	0.048	1.57	2	55	43
Herbs	0	0	0	0	0	0	0	0	0	0
Sparse vegetation	0	0	0	0	0	0	0	0	0	0
Sum land cover	4.99	0.09	0.03	2	0.63	0.1	2.1	3	53	45
Protected area	0.042	0	0	0.008	0	0	0.03	0	20	80
South America										
Rainfed agriculture	129	25	21	18	12	37	17	36	23	41
Irrigation	16	3	2.4	2.3	1.7	4	3	32	26	42
Grassland	201	23	23	40	32	37	46	23	35	41
Shrubs	259	36	23	83	40	35	43	23	47	30
Trees	992	60	54	190	283	88	316	12	48	41
Herbs	21	0.6	0.95	4	6	1.18	9	7	44	48
Sparse vegetation	41	0.3	0.28	15	18	0.17	7	1	81	18
Sum land cover	1659	148	124	352	392	202	441	16	45	39
Protected area	125	3	3	27	39	3	49	5	53	42

Deg = degradation; det = deterioration

	Total area (Mha)	Strong deg (Mha)	Light deg (Mha)	Strong det (Mha)	Light det (Mha)	Stable-high pressure (Mha)	Stable-low pressure (Mha)	Deg (%)	Det (%)	Stable (%)
South Asia										
Rainfed agriculture	108	33	22	12	8	23	9	51	19	30
Irrigation	92	48	10	14	5	10	5	63	21	16
Grassland	45	12	6	13	4	6	5	38	37	25
Shrubs	26	5	3	6	4	4	4	30	39	31
Trees	60	12	8	15	9	7	9	32	40	28
Herbs	0.7	0.03	0.003	0.11	0.02	0	0.56	4	18	78
Sparse vegetation	4	0.32	0.05	3	0.77	0.06	0.17	8	87	5
Sum land cover	337	109	49	63	31	51	34	47	28	25
Protected area	21	4	1.8	8	3	1.5	3	27	50	23
Southeast Asia										
Rainfed agriculture	88	20	14	14	11	16	13	39	29	32
Irrigation	22	6	3	4	3	4	3	41	28	31
Grassland	28	5	4	5	4	4	5	32	34	34
Shrubs	43	6	4	8	8	6	11	24	38	39
Trees	280	31	19	84	61	21	64	18	52	30
Herbs	0.92	0.19	0.18	0.25	0.12	0.1	0.08	40	41	20
Sparse vegetation	0.03	0.007	0.006	0.001	0.005	0.005	0.002	52	24	24
Sum land cover	462	67	45	115	88	51	95	24	44	32
Protected area	53	4	2.3	21	13	2.2	12	11	63	26
Sub-Saharan Africa										
Rainfed agriculture	227	31	40	23	33	53	46	32	25	44
Irrigation	7	1	1.3	1.1	1.3	1.4	1.3	30	33	37
Grassland	465	25	32	76	97	57	178	12	37	50
Shrubs	452	31	43	87	106	53	132	16	43	41
Trees	687	52	56	158	200	52	169	16	52	32
Herbs	15	1.1	1.2	2.4	3	2.2	5	15	36	49
Sparse vegetation	55	0.44	0.9	4	16	3	30	2	37	61
Sum land cover	1909	142	175	351	457	222	562	17	42	41
Protected area	207	13	17	39	44	30	64	14	40	46

Deg = degradation; det = deterioration

	Total area (Mha)	Strong deg (Mha)	Light deg (Mha)	Strong det (Mha)	Light det (Mha)	Stable-high pressure (Mha)	Stable-low pressure (Mha)	Deg (%)	Det (%)	Stable (%)
West Asia										
Rainfed agriculture	34	12	6	4	1.7	8	2.5	52	17	31
Irrigation	23	10	3	4	1.3	3	1	60	23	17
Grassland	27	10	4	4	2	5	2.2	50	23	27
Shrubs	61	25	6	19	6	2.1	3	50	42	8
Trees	39	8	5	4	3	13	7	34	16	50
Herbs	6	1.4	0.1	4	0.31	0.07	0.08	26	71	3
Sparse vegetation	31	10	4	9	5	3	2.4	42	42	16
Sum land cover	223	77	27	47	19	35	17	47	30	23
Protected area	4	1.3	0.46	1.3	0.6	0.34	0.24	43	44	14
West & Central Europe										
Rainfed agriculture	103	3	10	1.6	4	73	11	12	6	82
Irrigation	19	0.9	2.5	0.6	1.4	9	4	18	11	71
Grassland	69	2.1	10	1.2	2.3	46	7	17	5	78
Shrubs	25	0.7	1.6	4	2.4	5	12	9	25	66
Trees	192	3	14	1.9	6	123	44	9	4	87
Herbs	11	0.057	0.41	0.62	0.47	4	6	4	10	86
Sparse vegetation	14	0.2	0.69	1.5	0.66	1.7	9	7	16	78
Sum land cover	433	10	39	11	17	262	93	11	7	82
Protected area	57	1.6	5	1.7	3	28	17	11	9	80
World										
Rainfed agriculture	1212	165	175	96	115	420	240	28	17	54
Irrigation	315	96	42	34	22	79	41	44	18	38
Grassland	1910	118	128	276	366	294	728	13	34	54
Shrubs	1438	119	99	285	299	158	478	15	41	44
Trees	4335	225	260	579	883	752	1636	11	34	55
Herbs	203	7	9	16	35	24	111	8	25	67
Sparse vegetation	1034	37	48	225	274	74	376	8	48	44
Sum land cover	10448	769	761	1512	1994	1801	3611	15	34	52
Protected area	880	34	41	170	192	103	340	9	41	50

Deg = degradation; det = deterioration

	Total area (Mha)	Strong deg (Mha)	Light deg (Mha)	Strong det (Mha)	Light det (Mha)	Stable-high pressure (Mha)	Stable-low pressure (Mha)	Deg (%)	Det (%)	Stable (%)
High income										
Rainfed agriculture	359	30	34	16	18	167	94	18	10	73
Irrigation	54	7	7	4	4	20	11	27	15	58
Grassland	427	24	31	62	67	98	145	13	30	57
Shrubs	421	25	14	100	98	29	155	9	47	44
Trees	1081	53	81	103	133	348	363	12	22	66
Herbs	88	4	6	5	13	17	44	11	20	69
Sparse vegetation	734	18	32	176	206	45	257	7	52	41
Sum land cover	3164	161	205	466	538	723	1070	12	32	57
Protected area	286	9	12	54	56	43	112	7	39	54
Upper middle income										
Rainfed agriculture	399	49	60	31	44	141	74	27	19	54
Irrigation	128	32	18	12	9	37	19	39	17	44
Grassland	1001	58	57	153	216	127	389	12	37	52
Shrubs	544	55	34	112	104	64	173	16	40	44
Trees	2179	81	93	230	469	302	1003	8	32	60
Herbs	94	2.2	1.9	8	18	5	59	4	28	68
Sparse vegetation	178	16	13	29	42	21	57	16	40	44
Sum land cover	4523	295	278	576	903	698	1774	13	33	55
Protected area	317	9	9	48	80	26	145	6	40	54
Lower middle income										
Rainfed agriculture	326	63	60	34	36	88	44	38	22	41
Irrigation	122	54	16	16	8	19	10	57	20	23
Grassland	227	22	22	25	33	40	85	19	26	55
Shrubs	211	19	24	29	43	33	63	20	34	46
Trees	640	56	50	145	155	64	170	17	47	37
Herbs	8	0.24	0.2	0.88	1.6	0.36	5	5	31	64
Sparse vegetation	68	0.76	1.6	2.3	11	6	47	3	19	77
Sum land cover	1601	214	174	253	287	251	422	24	34	42
Protected area	151	10	11	33	32	17	47	14	43	42

Deg = degradation; det = deterioration

	Total area (Mha)	Strong deg (Mha)	Light deg (Mha)	Strong det (Mha)	Light det (Mha)	Stable-high pressure (Mha)	Stable-low pressure (Mha)	Deg (%)	Det (%)	Stable (%)
Low income										
Rainfed agriculture	132	24	21	15	17	25	29	34	25	41
Irrigation	12	3	1.2	1.8	1.4	2.3	2.1	36	27	37
Grassland	255	14	18	32	50	31	110	13	32	55
Shrubs	266	20	27	43	56	32	87	18	37	45
Trees	440	34	37	101	127	40	101	16	52	32
Herbs	13	1.1	1.2	3	3	2	4	17	38	45
Sparse vegetation	38	1.8	1.5	3	14	3	15	8	44	47
Sum land cover	1157	99	107	197	269	137	349	18	40	42
Protected area	113	7	9	21	23	17	36	14	39	47
Low income & food deficit										
Rainfed agriculture	183	30	32	19	25	40	38	34	24	42
Irrigation	25	8	4	2.1	2	5	4	47	17	36
Grassland	337	18	25	37	62	44	150	13	29	58
Shrubs	327	23	35	50	69	43	107	18	36	46
Trees	552	40	46	127	158	52	129	16	52	33
Herbs	15	1.1	1.2	3	3	2.1	5	16	39	45
Sparse vegetation	58	2	2.2	3	16	5	29	7	34	59
Sum land cover	1495	122	145	241	335	190	460	18	39	44
Protected area	136	8	12	27	29	19	41	15	41	44
Least developed										
Rainfed agriculture	167	26	28	18	23	35	38	32	24	43
Irrigation	19	6	3	2.3	2.1	3	3	49	23	28
Grassland	325	17	23	34	59	42	150	12	29	59
Shrubs	340	25	34	52	74	42	114	17	37	46
Trees	605	47	51	130	172	47	158	16	50	34
Herbs	15	1.2	1.3	3	3	2.1	4	17	38	45
Sparse vegetation	50	1.3	1.5	3	15	3	26	6	37	58
Sum land cover	1522	124	142	242	348	174	492	17	39	44
Protected area	144	9	11	25	28	23	48	14	37	49

This report serves as background for the State of Land and Water Resources for Food and Agriculture (SOLAW 21). It provides updated information on the global distribution of land degradation and areas at risk, with special attention to agricultural land and forest. The applied methodology is described, and the results and caveats of the study are presented for readers that want a deeper understanding of the topic.

ISBN 978-92-5-137166-4

9 789251 371664

CC2843EN/1/11.23